Propagation of hybrid uncertainty by synthesizing B-spline chaos and augmented change of probability measure

Wan, Zhiqiang; Tao, Weifeng; Wang, Xiuli; Gao, Yuan

DOI
10.1016/j.strusafe.2024.102524

Publication date
2024

Document Version
Final published version

Published in
Structural Safety

Citation (APA)
Wan, Z., Tao, W., Wang, X., & Gao, Y. (2024). Propagation of hybrid uncertainty by synthesizing B-spline chaos and augmented change of probability measure. *Structural Safety*, *111*, Article 102524. https://doi.org/10.1016/j.strusafe.2024.102524

Structural Safety 111 (2024) 102524

Contents lists available at ScienceDirect

Structural Safety

journal homepage: www.elsevier.com/locate/strusafe

Propagation of hybrid uncertainty by synthesizing B-spline chaos and augmented change of probability measure

Zhiqiang Wan [a,*], Weifeng Tao [a], Xiuli Wang [b,c], Yuan Gao [a]

[a] School of Mechanics, Civil Engineering and Architecture, Northwestern Polytechnical University, Xi'an 710072, PR China
[b] Biobased Structures and Materials, Faculty of Civil Engineering and Geosciences, Delft University of Technology, Delft 2628 BL, The Netherlands
[c] Institute of Bio- and Geosciences, IBG-2: Plant Sciences, Forschungszentrum Jülich GmbH, Jülich 52425, Germany

ARTICLE INFO

Keywords:
Uncertainty quantification
Hybrid uncertainty propagation
B-spline chaos
Change of probability measure

ABSTRACT

Acquiring engineering data is frequently expensive, resulting in sparse data that may lead to a lack of knowledge for design and analysis. Thus, it is not always feasible to precisely determine the probability density functions (PDFs) of uncertain model parameters. Under such circumstances that involve simultaneous aleatory and epistemic uncertainties, repeated uncertainty propagation (UP) analysis is generally required. In this paper, a novel approach for hybrid UP is proposed by integrating B-spline chaos and augmented change of probability measure (aCOM) for meeting different goals. The B-spline chaos is adopted to represent the complicated computational model as a function of an arbitrary input random variable, while the aCOM is employed to reconstruct the PDF of the model output when the input PDF is changed due to epistemic uncertainty. In the case of small epistemic uncertainty, hybrid UP can be achieved directly by changing the assigned probabilities of existing sample results. While in the case of large epistemic uncertainty, additional samples from an augmenting PDF are generated. The proposed method is compatible with both cases. The numerical algorithm of the proposed method is presented and illustrated by four benchmark problems. Further, the accuracy and efficiency of the proposed method are substantiated by four numerical examples compared with analytical solutions or Monte Carlo simulations. An attempt to enhance the proposed method with the aid of active subspace methods to handle high-dimensional problems is also discussed in this work. The limitations and potential improvements of the proposed approach are outlined as well.

1. Introduction

1.1. Context of the paper

The utilization of computational models to aid in the development of practical engineering methods has emerged as a critical approach for addressing engineering challenges across various fields. Nevertheless, as a result of the intricate nature of real-world issues, the predictive analytical outcomes of most computational models may still exhibit significant uncertainty, which can be classified into two overarching categories [1–4]: (1) *aleatory uncertainty* (due to natural variation) and (2) *epistemic uncertainty* (due to lack of knowledge).

In general, the aleatory uncertainty can be characterized by precisely specifying the probability density functions (PDFs) of input random variables, while the epistemic uncertainty can be quantified through non-probabilistic ways such as interval analysis [5], augmented first-order reliability method [6], and operator norm-based approach [7]. Specially, if only the statistical aspect is considered, epistemic uncertainty can also be described in a probabilistic framework, e.g., by adopting imprecise probability models [8]. Particularly, it is possible for both of the aforementioned forms of uncertainties to coexist concurrently. Therefore, a more comprehensive approach is to consider them as hybrid uncertainty or polymorphic uncertainty [9].

In a study of engineering decision-making problems under the two types of uncertainties, Faber [10] has pointed out that the combination of simple physical models and hybrid uncertainty may be more suitable for describing uncertainty phenomena than applying complex physical models with a large number of parameters. Besides, research by Der Kiureghian and Ditlevsen [2] also indicated that if various types of uncertainties are not distinguished or even misjudged, the structural failure probability may be significantly overestimated or underestimated, and even deviate by several orders of magnitude in some cases.

* Corresponding author.
E-mail addresses: wanzhiqiang@nwpu.edu.cn (Z. Wan), wftao2048@nwpu.edu.cn (W. Tao), xiu.wang@fz-juelich.de (X. Wang), gaoyuan1@mail.nwpu.edu.cn (Y. Gao).

https://doi.org/10.1016/j.strusafe.2024.102524
Received 26 March 2024; Received in revised form 11 July 2024; Accepted 22 August 2024
Available online 27 August 2024

To this end, in the present paper, the primary focus is on hybrid uncertainty, with particular attention given to the challenging problem of hybrid uncertainty propagation. One specific engineering practice is that the probabilistic models of input random variables cannot be perfectly obtained by engineers at the initial stage of design. For this engineering scenario, it is typically required to reevaluate the design if these probabilistic models are updated (possibly more than once), incurring massive computational costs. To solve this issue, a wide range of methodologies have been developed, such as sparse polynomial chaos expansion [11], resampling Monte Carlo simulation [12], probability density evolution method integrated with change of probability measure [4] and its improvements [13], and more can be found in [14].

Despite variations in fundamental theories, almost all of these methods share a similar characteristic, viz., hybrid uncertainty propagation relies on two key aspects: (i) an accurate method for aleatory uncertainty propagation and (ii) an effective technique to reuse existing analysis results as many as possible. Correspondingly, there are at least two challenging issues involved: (1) how to accurately cope with high-dimensional random variables, and (2) how to efficiently deal with limited information. Although the former seems more challenging, this work aims to provide new insights on the latter.

1.2. Novelty of the paper

A novel approach is proposed for hybrid uncertainty propagation according to the above two aspects. The implementation of the proposed method is based on two state-of-the-art methods, i.e., the B-spline chaos [15] developed by Eckert et al. and Rahman [16] independently (to the best of authors' knowledge), for the first aspect, and the augmented change of probability measure (aCOM) [13] by the authors for the second one. It should be emphasized that B-spline chaos may not be the only option in this work, but it is found to cooperate well with the aCOM, especially in convenience of numerical analysis. Besides, the study in [15] indicates that B-spline chaos generalizes the Legendre multi-element chaos [17], and low-order B-spline chaos may yield more accurate results than a high-order polynomial chaos expansion for non-smooth functions [16]. All these specific advantages of B-spline chaos show the potential of the current work.

The proposed method is advantageous in three aspects: (1) computational cost for hybrid uncertainty quantification can be pre-estimated; (2) no assumptions are made about the linearity of computational models or the degree of epistemic uncertainty involved; and (3) the two adopted methods are not coupled, thus any individual improvements to the B-spline chaos and aCOM may promote the proposed approach.

1.3. Organization of the paper

In Section 2 the newly developed B-spline chaos is first revisited. An efficient method for constructing the B-spline chaos is also proposed in this section. The change of probability measure and its improvement called as aCOM are briefly discussed in Section 3. The proposed method is illustrated subsequently in Section 4 from theoretical aspect and is verified by four benchmark problems. Four applications are studied to further evaluate the proposed method in Section 5 and concluding remarks are outlined in Section 6.

2. Propagation of aleatory uncertainty via B-spline chaos

2.1. Basic concepts and formulation

In this section, the basic concepts and formulation of B-spline chaos proposed by Eckert C., Beer M. and Spanos P.D. [15] are first revisited. Define the triple $(\Omega, \mathscr{F}, \mathbb{P})$ be the probability space, where Ω is the sample space, $\mathscr{F}$ is the event space (σ-algebra) and $\mathbb{P}$ is the probability measure. Let Θ be an arbitrary random variable on $(\Omega, \mathscr{F}, \mathbb{P})$ and define by $L_2(\Omega, \mathscr{F}, \mathbb{P})$ the Hilbert space. Without loss of generality, consider a parametric model with the random parameter Θ, i.e.,

$$X = g(\Theta), \tag{1}$$

where X is the quantity of interest (QoI) and the mapping $g(\cdot) : \mathbb{R}^1 \mapsto \mathbb{R}^1$ is defined to be square-integrable. Note that $g(\cdot)$ is deterministic and measurable, and can be either explicit (e.g., via analytical formulation) or implicit (e.g., via finite element method).

If the distribution of Θ is precisely known, e.g., the probability density function (PDF) $p_\Theta(\theta)$ is clearly defined, it is known that calculating the PDF of X defined by $p_X(x)$ becomes a typical issue of propagation of aleatory uncertainty. Among various methods for propagation of aleatory uncertainty as mentioned in Section 1, we introduce the B-spline chaos [15] to represent Eq. (1), i.e.,

$$X \approx \tilde{X}_{n,p} = \sum_{i=1}^{n} b_i B_{i,p}(u(\Theta)), \tag{2}$$

where $B_{i,p}(u)$ is the ith B-spline basis function of order p defined with $u \in [0,1]$ for $i = 1, \ldots, n$, n is the number of B-spline basis functions and b_i is the ith B-spline coefficient. Herein $u(\cdot)$ should be a bijective function that uniquely maps Θ on the parametric space $[0,1]$. As suggested in [15], a natural choice is to adopt the cumulative distribution function (CDF) of Θ, i.e., $u(\theta) = P_\Theta(\theta) = \int_{-\infty}^{\theta} p_\Theta(\tau)\mathrm{d}\tau$.

The B-spline basis functions are defined by the Cox–de Boor recursion formula starting with piecewise constants for $p = 0$, i.e., $B_{i,0}(u) = 1$ if $u \in [\xi_i, \xi_{i+1})$, otherwise $B_{i,0}(u) = 0$, and for $p = 1, 2, \ldots$, there is

$$B_{i,p}(u) = \frac{u - \xi_i}{\xi_{i+p} - \xi_i} B_{i,p-1}(u) + \frac{\xi_{i+p+1} - u}{\xi_{i+p+1} - \xi_{i+1}} B_{i+1,p-1}(u), \tag{3}$$

where $\xi_i \in \mathbb{R}^1$ is the ith knot belonging to the knot vector $\Xi = \{\xi_1, \xi_2, \ldots, \xi_{n+p+1}\}$ for $\xi_i \le \xi_{i+1}$ and $i = 1, 2, \ldots, n+p+1$. Note that the form 0/0 is defined to be zero [18]. In general, the knot vector is defined to be open and normalized, namely, its first and last knots are repeated for $p+1$ times and $\xi_i \in [0,1]$, e.g., $\Xi = \{0,0,0,0.2,0.4,0.6,0.8,1,1,1\}$ ($p = 2$ and $n = 7$), $\Xi = \{0,0,0,0,0,0.5,1,1,1,1,1\}$ ($p = 4$ and $n = 6$), etc. The B-spline basis functions for the above two knot vectors are drawn in Figs. 1(a) and 1(b), respectively.

According to the proof in [15], $\tilde{X}_{n,p}$ defined in Eq. (2) can be the weak B-spline chaos approximation of X if the B-spline coefficient vector $\boldsymbol{b} = [b_1, \ldots, b_n]^\top$ results from the L_2 projection $\mathbf{B}\mathbf{b} = \mathbf{x}$, in which

$$\mathbf{B}_{i,j} \overset{\text{def}}{=} \mathbb{E}[B_{i,p}(u(\Theta))B_{j,p}(u(\Theta))] \tag{4}$$

and

$$\mathbf{x}_j \overset{\text{def}}{=} \mathbb{E}[g(\Theta)B_{j,p}(u(\Theta))] \tag{5}$$

for $i, j = 1, \ldots, n$, where $\mathbf{B}_{i,j}$ locates in the ith-row-jth-column of $\mathbf{B}$, $\mathbf{x}_j$ is the jth entry of $\mathbf{x}$, and $\mathbb{E}[\cdot]$ is the expectation operator. Then the B-spline coefficients can be calculated via $\mathbf{b} = \mathbf{B}^{-1}\mathbf{x}$.

Remark 1. Note that $\mathbf{B}$ is a symmetric and band matrix in which $\mathbf{B}_{i,j} = 0$ for $|i-j| > p+1$ and $i, j = 1, 2, \ldots, n$. In other words, it is convenient to only calculate entries of $\mathbf{B}$ for $0 \le i - j \le p+1$. Besides, since $\mathbf{B}$ is only dependent on the utilization of B-spline basis functions and the PDF of Θ, one can resolve $\mathbf{B}$ effortlessly when p and n are increased in order to achieve the convergence of B-spline chaos.

2.2. Computation of B-spline coefficients via partition of probability-assigned space

The two integrals in Eqs. (4) and (5) can be computed numerically via Monte Carlo simulation (MCS), i.e.,

$$\begin{aligned}\mathbf{B}_{i,j} &= \mathbb{E}[B_{i,p}(u(\Theta))B_{j,p}(u(\Theta))] \\ &= \int_\Omega B_{i,p}(u(\theta))B_{j,p}(u(\theta))p_\Theta(\theta)\mathrm{d}\theta \\ &\approx \frac{1}{N}\sum_{q=1}^{N} B_{i,p}(u(\theta_q))B_{j,p}(u(\theta_q))\end{aligned} \tag{6}$$

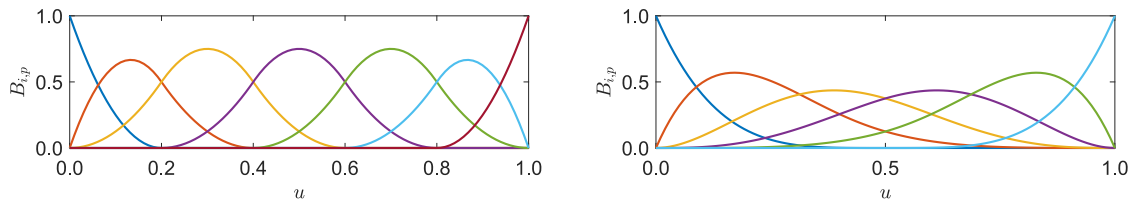

(a) $\Xi = \{0, 0, 0, 0.2, 0.4, 0.6, 0.8, 1, 1, 1\}$ (b) $\Xi = \{0, 0, 0, 0, 0, 0.5, 1, 1, 1, 1, 1\}$

Fig. 1. B-spline basis functions of orders $p = 2$ and $p = 4$ with $n = 7$ and $n = 6$, respectively.

and

$$\begin{aligned}\mathbf{x}_j &= \mathbb{E}[g(\Theta)B_{j,p}(u(\Theta))] \\ &= \int_{\Omega} g(\theta)B_{j,p}(u(\theta))p_{\Theta}(\theta)\mathrm{d}\theta \\ &\approx \frac{1}{N}\sum_{q=1}^{N} g(\theta_q)B_{j,p}(u(\theta_q)),\end{aligned} \tag{7}$$

where $\{\theta_q\}_{q=1}^{N} \sim p_{\Theta}(\theta)$ are MCS samples of size N.

In general, to ensure the accuracy of MCS, N should be large enough such as 10^5 or even 10^6. This is totally fine for calculating Eq. (6) since calculating $B_{i,p}$ needs almost no computational cost. Nevertheless, it is challenging to do the same for Eq. (7) due to the complexity of $g(\cdot)$ in mostly real engineering practices.

To this end, we introduce the GF-discrepancy minimization strategy [19] for determining a representative point set $\{\theta_q\}_{q=1}^{N} \sim p_{\Theta}(\theta)$ with the assigned probabilities $\{P_q\}_{q=1}^{N}$, which are defined by

$$P_q = \int_{\Omega_q} p_{\Theta}(\theta)\mathrm{d}\theta,\ q = 1, 2, \ldots, N, \tag{8}$$

where $\{\Omega_q\}_{q=1}^{N}$ is a partition of the distribution domain Ω of Θ, satisfying that $\cup_{q=1}^{N}\Omega_q = \Omega$ and $\Omega_p \cap \Omega_q = \emptyset$ for $\forall p \neq q$ and $p, q = 1, 2, \ldots, N$. Note that it is obvious that $\sum_{q=1}^{N} P_q = 1$ and $P_q \in [0, 1]$. One convenient choice to define the representative volume Ω_q is the Voronoi cell [20]:

$$\Omega_q \overset{\text{def}}{=} \left\{\theta \in \mathbb{R}^1 : \left|\theta - \theta_q\right| \leq \left|\theta - \theta_j\right| \text{ for } j = 1, 2, \ldots, N\right\}. \tag{9}$$

To do so, the numerical approximation of $\mathbf{B}_{i,j}$ and $\mathbf{x}_j$ becomes

$$\begin{aligned}\mathbf{B}_{i,j} &= \int_{\Omega} B_{i,p}(u(\theta))B_{j,p}(u(\theta))p_{\Theta}(\theta)\mathrm{d}\theta \\ &= \sum_{q=1}^{N}\int_{\Omega_q} B_{i,p}(u(\theta))B_{j,p}(u(\theta))p_{\Theta}(\theta)\mathrm{d}\theta \\ &\approx \sum_{q=1}^{N} B_{i,p}(u(\theta_q))B_{j,p}(u(\theta_q))P_q\end{aligned} \tag{10}$$

and

$$\begin{aligned}\mathbf{x}_j &= \int_{\Omega} g(\theta)B_{j,p}(u(\theta))p_{\Theta}(\theta)\mathrm{d}\theta \\ &= \sum_{q=1}^{N}\int_{\Omega_q} g(\theta)B_{j,p}(u(\theta))p_{\Theta}(\theta)\mathrm{d}\theta \\ &\approx \sum_{q=1}^{N} g(\theta_q)B_{j,p}(u(\theta_q))P_q.\end{aligned} \tag{11}$$

The numerical algorithm of the GF-discrepancy minimization strategy is summarized in Appendix A.

The benefits of Eqs. (10) and (11) are twofold: (1) Compared to MCS sample points, the representative point set has a lower GF-discrepancy for the same sample size N. See detailed discussions in [21,22], and the error analysis in the next section; (2) This provides convenience for extending the scope of B-spline chaos in uncertainty propagation from aleatory aspects to epistemic ones via change of probability measure [4,13]. We will prove it in Section 3.

2.3. Error analysis of calculation of B-spline chaos via GF-discrepancy minimization strategy

In [15], it has been proved that $\tilde{X}_{n,p}$ converges in probability and in distribution, and both [15,16] have studied the error of B-spline chaos approximation in terms of the number and order of B-spline basis functions. This section provides the error analysis of calculation of B-spline chaos via GF-discrepancy minimization strategy, which is important but has not been mentioned in the literature as yet.

As discussed above, if the number and order of B-spline basis functions are determined to be large enough, the numerical error of $\tilde{X}_{n,p}$ can be assumed to originate from the B-spline coefficient vector $\mathbf{b}$, which is calculated from the L_2 projection $\mathbf{Bb} = \mathbf{x}$. Note that the accuracy of $\mathbf{B}$ can be well satisfied by considering Eq. (6) with a large N, since $B_{i,p}$ is explicitly known. For this reason, the error estimate is focused on $\mathbf{x}$, or equivalently, its component $\mathbf{x}_j$ as defined in Eq. (11).

Recall the numerical approximation $\tilde{\mathbf{x}}_j$ of $\mathbf{x}_j$ given in Eq. (11):

$$\tilde{\mathbf{x}}_j = \sum_{q=1}^{N} g(\theta_q)B_{j,p}(u(\theta_q))P_q. \tag{12}$$

Then, the numerical error of estimating $\mathbf{x}_j$ can be defined by

$$\begin{aligned}\epsilon_j &\overset{\text{def}}{=} \left|\mathbf{x}_j - \tilde{\mathbf{x}}_j\right| \\ &= \left|\int_{\Omega} f_{j,p}(\theta)p_{\Theta}(\theta)\mathrm{d}\theta - \sum_{q=1}^{N} f_{j,p}(\theta_q)P_q\right|,\end{aligned} \tag{13}$$

where $f_{j,p}(\theta) \overset{\text{def}}{=} g(\theta)B_{j,p}(u(\theta))$. Further, the worst error defined in Eq. (13) can be estimated by the extended Koksma–Hlawka inequality [19,21], i.e.,

$$\left|\int_{\Omega} f_{j,p}(\theta)p_{\Theta}(\theta)\mathrm{d}\theta - \sum_{q=1}^{N} f_{j,p}(\theta_q)P_q\right| \leq 3.635\mathrm{TV}(f_{j,p})\mathcal{D}_{\mathrm{GF}}(\mathcal{M}), \tag{14}$$

where $\mathrm{TV}(f_{j,p})$ is the total variation of $f_{j,p}$, measuring the irregularity of $f_{j,p}$ in terms of its arguments, and $\mathcal{D}_{\mathrm{GF}}(\mathcal{M}) \in [0, 1]$ is the GF-discrepancy [19] of the point set $\mathcal{M} = \{\theta_q\}_{q=1}^{N}$.

From Eq. (14), it is now clear that, if we can generate a point set $\mathcal{M}$ that has a small GF-discrepancy, then the numerical error of $\mathbf{x}_j$ can be small as well. In other words, by taking the GF-discrepancy of the point set as a quantitative index, it is convenient to determine the number of sampling points needed for constructing the B-spline chaos. And on the contrary, if the sample size is fixed, the accuracy of B-spline chaos can be improved by design of these points to minimize the GF-discrepancy as well.

3. Propagation of epistemic uncertainty via change of probability measure

In this section, we consider a common situation that may happen in most engineering analysis – the PDF of Θ is imprecise rather than being precisely unknown, which belongs to the case of epistemic uncertainty in statistical aspect. For the sake of simplicity, let $p_{\Theta}^{(1)}(\theta)$ be a prior PDF of Θ and $p_{\Theta}^{(2)}(\theta)$ be an updated one, e.g., via Bayesian updating with

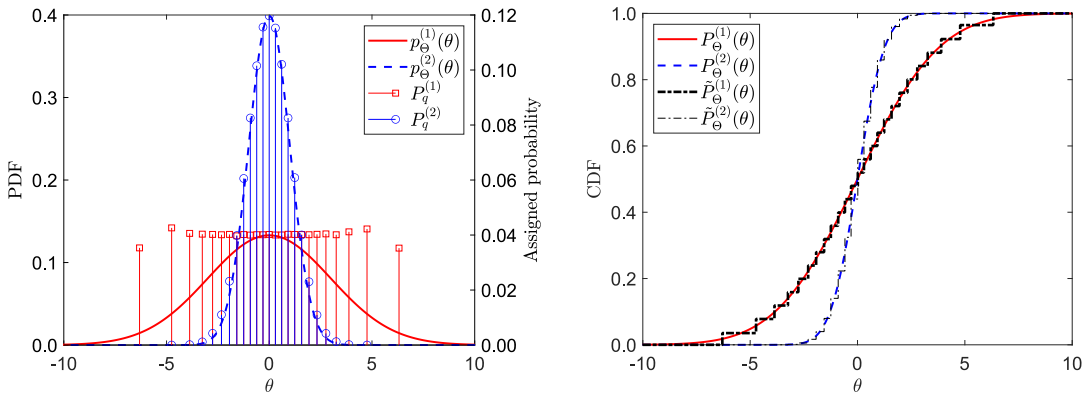

(a) PDF and assigned probabilities (b) CDF

Fig. 2. A simple case for the change of probability measure using $N = 25$ samples.

newly collected engineering data, and denote the PDF of X with respect to $p_\Theta^{(1)}(\theta)$ as $p_X^{(1)}(x)$ and the one in terms of $p_\Theta^{(2)}(\theta)$ by $p_X^{(2)}(x)$. Certainly, the B-spline chaos can be established individually for $p_\Theta^{(1)}(\theta)$ and $p_\Theta^{(2)}(\theta)$, but the number of samples will double from N to $2N$ simultaneously. To solve this issue, the change of probability measure (COM) [4] will be employed hereinafter.

3.1. Small epistemic uncertainty

We first consider the case of small epistemic uncertainty. Specifically, if $p_\Theta^{(2)}(\theta)$ is absolutely continuous with respect to $p_\Theta^{(1)}(\theta)$, namely, the support of $p_\Theta^{(1)}(\theta)$ completely covers the support of $p_\Theta^{(2)}(\theta)$, then the Radon–Nikodým theorem holds such that [23]

$$p_X^{(2)}(x) = \mathcal{T}_{\mathrm{RN}} \circ p_X^{(1)}(x), \tag{15}$$

where $\circ$ denotes the action of an operator on a function, and $\mathcal{T}_{\mathrm{RN}}$ is a measurable function (operator), the so-called Radon–Nikodým derivative of $p_\Theta^{(2)}(\theta)$ with respect to $p_\Theta^{(1)}(\theta)$. This means, one can directly obtain $p_X^{(2)}(x)$ by forcing the operator $\mathcal{T}_{\mathrm{RN}}$ on $p_X^{(1)}(x)$.

The Radon–Nikodým derivative $\mathcal{T}_{\mathrm{RN}}$ can be calculated via change of probability measure [4] as follows:

Step 1.1. For $\Theta \sim p_\Theta^{(1)}(\theta)$, select the point set denoted by $\mathcal{M}^{(1)} = \{\theta_q^{(1)}; P_q^{(1)}\}_{q=1}^N$ via the GF-discrepancy minimization strategy in Appendix A.

Step 1.2. For $\Theta \sim p_\Theta^{(2)}(\theta)$, define a new point set $\mathcal{M}^{(2)} = \{\theta_q^{(2)}; P_q^{(2)}\}_{q=1}^N$ with the same realizations of Θ in **Step 1.1**, i.e., $\theta_q^{(2)} = \theta_q^{(1)}$ for $q = 1, \ldots, N$, but recompute the assigned probabilities by

$$P_q^{(2)} = \int_{\Omega_q^{(1)}} p_\Theta^{(2)}(\theta)\mathrm{d}\theta, \ q = 1, 2, \ldots, N, \tag{16}$$

where $\Omega_q^{(1)}$ is the qth representative volume determined by $\{\theta_q^{(1)}\}_{q=1}^N$.

A simple case considering $p_\Theta^{(1)}(\theta) = \mathcal{N}(0, 3)$ and $p_\Theta^{(2)}(\theta) = \mathcal{N}(0, 1)$ is drawn in Fig. 2, where $\mathcal{N}(a, b)$ stands for the PDF of a normal random variable with mean value a and standard deviation b. From Fig. 2 it can be seen that the empirical CDF of Θ denoted by $\tilde{P}_\Theta^{(2)}(\theta)$ via COM fits well with the exact one.

3.2. Large epistemic uncertainty

What if the support of $p_\Theta^{(1)}(\theta)$ does not sufficiently cover the one of $p_\Theta^{(2)}(\theta)$? It should be emphasized that the "cover" herein should be understood as in numerical aspect rather than in mathematical aspect. For instance, considering $p_\Theta^{(1)}(\theta) = \mathcal{N}(0, 1)$ and $p_\Theta^{(2)}(\theta) = \mathcal{N}(8, 1)$, it is clear that although their mathematical supports are the same, i.e., $(-\infty, +\infty)$, the effective supports of the two PDFs having values far greater than zero are almost non-overlapping. A more practical example appears in life cycle assessment of structures considering the degradation of materials [24,25], in which the deteriorating elastic modulus is characterized by $E(t) = (1\text{–}0.007\ t^{0.85})E_0$. This means the mean value of elastic modulus may be decreased by 19.46% at the 50th year compared to the initial design stage, resulting in a large shift of the PDF of elastic modulus.

For such case of large epistemic uncertainty, the accuracy of COM may decrease sharply. The reason is intuitive: the lager the region where $p_\Theta^{(1)}(\theta)$ and $p_\Theta^{(2)}(\theta)$ do not overlap, the more representative points corresponding to the region will be equipped with $P_q^{(2)}$ of 0 on the definition of Eq. (16). Rigorously, this is because the Radon–Nikodým theorem cannot be strictly applied due to the lack of absolute continuity.

To solve this issue, an augmenting approach [13] was proposed recently to promote the accuracy of COM throughout a relatively low computational cost. The basic idea is to add some extra points to the original representative point set, such that the new point set conforms to the new distribution $p_\Theta^{(2)}(\theta)$.

The numerical algorithm of the augmented COM (aCOM) [13] is summarized as follows:

Step 2.1. Define $\Omega^{(1)}$ and $\Omega^{(2)}$ be the supports of $p_\Theta^{(1)}(\theta)$ and $p_\Theta^{(2)}(\theta)$, respectively, and $\Omega = \Omega^{(1)} \cup \Omega^{(2)}$ be the total support. Compute $\Omega_{\mathrm{IS}}^{(1)} = \{\theta; Q^{(1)}(0.025) \le \theta \le Q^{(1)}(0.975), \theta \in \Omega\}$ where $Q^{(1)}(\cdot)$ is the quantile function with respect to $p_\Theta^{(1)}(\theta)$. Let $\Omega_+ = \{\theta; p_\Theta^{(2)}(\theta) \ge p_\Theta^{(1)}(\theta), \theta \in \Omega\}$, $\Omega_{\mathrm{aug}} = \Omega_+ \backslash \Omega_{\mathrm{IS}}^{(1)}$, and compute

$$\pi_a^{(1)} = \int_{\Omega_{\mathrm{aug}}} p_\Theta^{(1)}\mathrm{d}\theta \ \text{ and } \ \pi_a^{(2)} = \int_{\Omega_{\mathrm{aug}}} p_\Theta^{(2)}\mathrm{d}\theta. \tag{17}$$

Step 2.2. Generate the augmenting distribution $p_\Theta^{(\mathrm{aug})}(\theta)$ by

$$p_\Theta^{(\mathrm{aug})}(\theta) = \frac{p_\Theta^{(2)}(\theta) - p_\Theta^{(1)}(\theta)}{\pi_a^{(2)} - \pi_a^{(1)}}, \ \theta \in \Omega_{\mathrm{aug}}. \tag{18}$$

Step 2.3. Generate $N_{\mathrm{aug}} = \lceil \Delta\pi \cdot N \rceil$ samples denoted by $\{\theta_q^{\mathrm{aug}}\}_{q=1}^{N_{\mathrm{aug}}}$ from the augmenting distribution $p_\Theta^{(\mathrm{aug})}(\theta)$, where $\Delta\pi = \pi_a^{(2)} - \pi_a^{(1)}$. Define the new representative points $\{\theta_q^{(2)}\}_{q=1}^{N+N_{\mathrm{aug}}}$ satisfying that

$$\theta_q^{(2)} = \begin{cases} \theta_q^{(1)} \ \text{for } q = 1, \ldots, N, \\ \theta_{q-N}^{\mathrm{aug}} \ \text{for } q = N+1, \ldots, N+N_{\mathrm{aug}}. \end{cases} \tag{19}$$

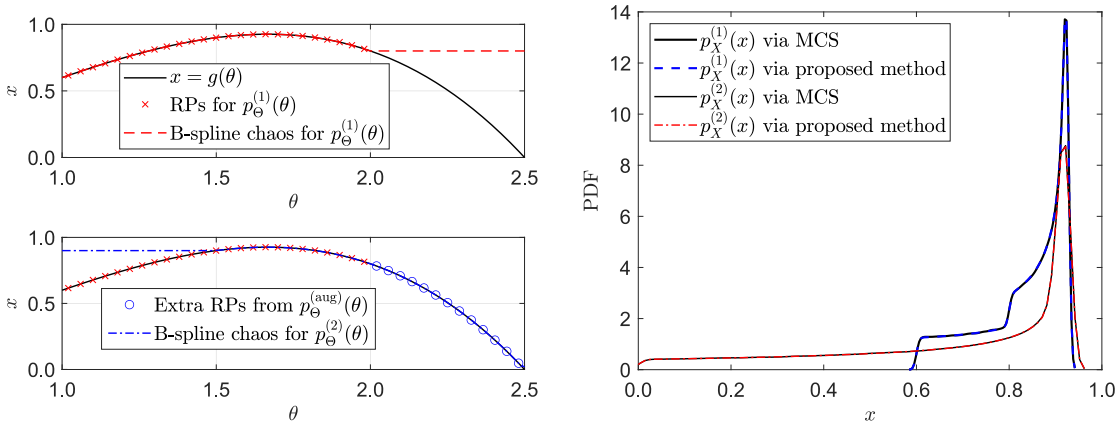

(a) Using B-spline chaos for prediction

(b) PDFs of $p_X^{(1)}(x)$ and $p_X^{(2)}(x)$

Fig. 3. Illustration of prediction results via B-spline chaos. RPs: representative points. Calculation setup parameters: $N = 25$, $N_{\mathrm{aug}} = 13$, $p = 5$, and $n = 10$.

Step 2.4. Calculate the changed assigned probabilities by

$$P_q^{(2)} = \int_{\Omega_q^{(2)}} p_\Theta^{(2)}(\theta)\mathrm{d}\theta,\ q = 1, 2, \ldots, N + N_{\mathrm{aug}}, \tag{20}$$

where $\Omega_q^{(2)}$ is the qth representative volume determined by $\{\theta_q^{(2)}\}_{q=1}^{N+N_{\mathrm{aug}}}$. For the sake of lengthiness, the proof that the point set $\{\theta_q^{(2)}\}_{q=1}^{N+N_{\mathrm{aug}}}$ via aCOM follows the distribution $p_\Theta^{(2)}(\theta)$ is given in Appendix B.

Remark 2. If $\Omega_{\mathrm{aug}} = \emptyset$ (e.g., the two PDFs in Fig. 2(a)), then $\pi_a^{(1)} = \pi_a^{(2)} = 0$ and $N_{\mathrm{aug}} = 0$, which means there is no need to add extra points. This situation degenerates into the case of small epistemic uncertainty in Section 3.1, i.e., aCOM → COM. On the contrary, if $\Omega_{\mathrm{aug}} = \Omega_+$, viz., there is no overlapped region between $p_\Theta^{(1)}(\theta)$ and $p_\Theta^{(2)}(\theta)$, then $\pi_a^{(1)} = 0$, $\pi_a^{(2)} = 1$, and $N_{\mathrm{aug}} = N$, which means one should repeat a complete analysis of aleatory uncertainty propagation, i.e., a specific situation of large epistemic uncertainty. To this end, the pre-estimated index $\Delta\pi \in [0, 1]$ can be adopted to judge whether small or large epistemic uncertainty is present. In conclusion, the aCOM is available in both cases of small and large epistemic uncertainties. Therefore, only the aCOM is employed in the following analysis.

4. The proposed method for hybrid uncertainty propagation

4.1. Theoretical illustration

The proposed method for hybrid uncertainty propagation is based on the aforementioned B-spline chaos and aCOM. Assume $\Theta^{(1)} \sim p_\Theta^{(1)}(\theta)$ and $\Theta^{(2)} \sim p_\Theta^{(2)}(\theta)$ where the CDFs of $\Theta^{(1)}$ and $\Theta^{(2)}$ are denoted by $P_\Theta^{(1)}(\theta)$ and $P_\Theta^{(2)}(\theta)$, respectively. Recall that the mapping $g(\cdot)$ in Eq. (1) is unchanged but the PDF of Θ may be imprecise. Then, two B-spline chaos approximations can be generated by

$$X^{(1)} \approx \tilde{X}_{n,p}^{(1)} = \sum_{i=1}^{n} b_i^{(1)} B_{i,p}\left(P_\Theta^{(1)}(\theta)\right),\ \Theta = \Theta^{(1)} \sim p_\Theta^{(1)}(\theta), \tag{21a}$$

$$X^{(2)} \approx \tilde{X}_{n,p}^{(2)} = \sum_{i=1}^{n} b_i^{(2)} B_{i,p}\left(P_\Theta^{(2)}(\theta)\right),\ \Theta = \Theta^{(2)} \sim p_\Theta^{(2)}(\theta), \tag{21b}$$

where we assume n and p are the same for the two B-spline chaos. It should be emphasized that it is not necessary to fix the order and the number of B-spline basis functions in the two B-spline chaos. The purpose of doing this herein is just to facilitate the explanation of the proposed method.

Now we consider the L_2 projection results of the B-spline chaos coefficients of Eqs. (21a) and (21b) via partition of probability-assigned space introduced in Section 2.2.

(1) For $X^{(1)}$ in terms of $\Theta^{(1)} \sim p_\Theta^{(1)}(\theta)$, we have $\mathbf{B}^{(1)}\mathbf{b}^{(1)} = \mathbf{x}^{(1)}$, where

$$\begin{aligned}\mathbf{B}_{i,j}^{(1)} &= \int_\Omega B_{i,p}\left(P_\Theta^{(1)}(\theta)\right) B_{j,p}\left(P_\Theta^{(1)}(\theta)\right) p_\Theta^{(1)}(\theta)\mathrm{d}\theta \\ &\approx \sum_{q=1}^{N_1} B_{i,p}\left(P_\Theta^{(1)}(\theta_q^{(1)})\right) B_{j,p}\left(P_\Theta^{(1)}(\theta_q^{(1)})\right) P_q^{(1)}\end{aligned} \tag{22}$$

and

$$\begin{aligned}\mathbf{x}_j^{(1)} &= \int_\Omega g(\theta) B_{j,p}\left(P_\Theta^{(1)}(\theta)\right) p_\Theta^{(1)}(\theta)\mathrm{d}\theta \\ &\approx \sum_{q=1}^{N_1} g(\theta_q^{(1)}) B_{j,p}\left(P_\Theta^{(1)}(\theta_q^{(1)})\right) P_q^{(1)}\end{aligned} \tag{23}$$

for $i, j = 1, \ldots, n$, where the representative point set is selected as $\{\theta_q^{(1)}; P_q^{(1)}\}_{q=1}^{N_1} \sim p_\Theta^{(1)}(\theta)$.

(2) Similarly, for $X^{(2)}$ in terms of $\Theta^{(2)} \sim p_\Theta^{(2)}(\theta)$, define $\mathbf{B}^{(2)}\mathbf{b}^{(2)} = \mathbf{x}^{(2)}$ and for $i, j = 1, \ldots, n$, we have

$$\begin{aligned}\mathbf{B}_{i,j}^{(2)} &= \int_\Omega B_{i,p}\left(P_\Theta^{(2)}(\theta)\right) B_{j,p}\left(P_\Theta^{(2)}(\theta)\right) p_\Theta^{(2)}(\theta)\mathrm{d}\theta \\ &\approx \sum_{q=1}^{N_2} B_{i,p}\left(P_\Theta^{(2)}(\theta_q^{(2)})\right) B_{j,p}\left(P_\Theta^{(2)}(\theta_q^{(2)})\right) P_q^{(2)}\end{aligned} \tag{24}$$

and

$$\begin{aligned}\mathbf{x}_j^{(2)} &= \int_\Omega g(\theta) B_{j,p}\left(P_\Theta^{(2)}(\theta)\right) p_\Theta^{(2)}(\theta)\mathrm{d}\theta \\ &\approx \sum_{q=1}^{N_2} g(\theta_q^{(2)}) B_{j,p}\left(P_\Theta^{(2)}(\theta_q^{(2)})\right) P_q^{(2)},\end{aligned} \tag{25}$$

where the representative point set is defined as $\{\theta_q^{(2)}; P_q^{(2)}\}_{q=1}^{N_2} \sim p_\Theta^{(2)}(\theta)$.

Let $N_1 = N_2 = N$ be sufficient large to ensure the accuracy of the two B-spline chaos. From Eqs. (23) and (25), it is known that a total number of $2N$ runs of $g(\cdot)$ is generally required to form the two B-spline chaos. However, if we adopt the aCOM introduced in Section 3, the computational cost decreases to $N + N_{\mathrm{aug}} \le 2N$ since $0 \le N_{\mathrm{aug}} \le N$. In other words, the efficiency of hybrid uncertainty propagation by the original B-spline chaos method can be improved by a maximum factor of 2.

Remark 3. Can we regard the B-spline chaos in Eq. (21a) as the metamodel (a.k.a. surrogate model) of $x = g(\theta)$ in Eq. (1)? If we can, perhaps the easiest way to obtain $p_X^{(2)}(x)$ is to conduct the MCS

using samples from $p_{\Theta}^{(2)}(\theta)$. The answer depends on the specific forms of $p_{\Theta}^{(1)}(\theta)$ and $p_{\Theta}^{(2)}(\theta)$, and is generally no, especially in the case of large epistemic uncertainty. A specific case is shown in Fig. 3, where we take $x = \theta^2 - 0.4\theta^3$, $p_{\Theta}^{(1)}(\theta) = \mathcal{U}(1.0, 2.0)$ and $p_{\Theta}^{(2)}(\theta) = \mathcal{U}(1.5, 2.5)$, where $\mathcal{U}(a, b)$ means the PDF of an uniform random variable in $[a, b]$. From Fig. 3(a), it can be seen that the B-spline chaos for $p_{\Theta}^{(1)}(\theta)$ can only work accurately in $[1.0, 2.0]$, while it fails outside of this region. Hence, for $p_{\Theta}^{(2)}(\theta)$ that has a different support of $[1.5, 2.5]$ the B-spline chaos needs to be reconstructed, e.g., via the proposed method. Notice that there is no information available for $x = g(\theta)$ with $\theta \in [2.0, 2.5]$, thus extra points of Θ should be analyzed. In other words, although B-spline chaos may work well for the problem that $x = g(\theta)$ with $\theta \in [1.0, 2.0]$, it may fail (without any change of the method) for another problem, see $x = g(\theta)$ with $\theta \in [2.0, 2.5]$. This phenomenon has been deeply discussed in [26] by using the *no-free-lunch* (NFL) theorem, where it states that "if an algorithm performs well on a certain class of problems, then, according to NFL, it necessarily will perform poorly on the set of all remaining problems". For this toy example, the PDF results via the proposed method are consistent with the MCS using 10^6 samples and kernel density estimation (KDE), as shown in Fig. 3(b). However, we want to stress that the proposed method may also not work efficiently for some situations according to NFL. This will be discussed in detail in the following section.

4.2. Numerical illustration

The numerical algorithm of the proposed approach is outlined in form of pseudo codes in Algorithm 1. Note that for high-dimensional cases, e.g., $\boldsymbol{\Theta} \in \mathbb{R}^s$ where $s \geq 2$, one can adopt the active subspace method [27] to first detect a one-dimensional active subspace (see Appendix C). Then, the proposed algorithm can still be valid and operated in this one-dimensional active subspace.

In this section, the versatility of the proposed approach is verified by considering four specific examples, in which the first two are commonly-used benchmark problems, the third shows how to apply the proposed method with the aid of dimension reduction techniques, and the last is designed to illustrate to the reader when the accuracy of the proposed method may deteriorate. More general and practical applications will be demonstrated in Section 5. During the following analysis, if no special parameters are determined, we set $N = 200$, $p = 10$ and $n = 30$.

4.2.1. Basic distributions

The first specific example considers $X = \Theta$, thus X has the same PDF as Θ. Specifically, we consider 10 different cases, where the first 5 cases study the change of mean value and standard deviation in the Normal distribution, while the last 5 cases consider changes among different configurations of distribution.

For the Case 1 to Case 5, let $p_{\Theta}^{(1)}(\theta) = \mathcal{N}(0.0, 1.0)$ be the prior PDF of Θ, while the new PDF $p_{\Theta}^{(2)}(\theta)$ is:

- Case 1: A small shift in mean value – $p_{\Theta}^{(2)}(\theta) = \mathcal{N}(0.2, 1.0)$,
- Case 2: A large shift in mean value – $p_{\Theta}^{(2)}(\theta) = \mathcal{N}(1.2, 1.0)$,
- Case 3: Narrowed standard deviation – $p_{\Theta}^{(2)}(\theta) = \mathcal{N}(0.0, 0.5)$,
- Case 4: Enlarged standard deviation – $p_{\Theta}^{(2)}(\theta) = \mathcal{N}(0.0, 2.5)$,
- Case 5: A large shift in mean value with enlarged standard deviation – $p_{\Theta}^{(2)}(\theta) = \mathcal{N}(1.2, 2.5)$.

The results of Case 1 to Case 5 are presented in Fig. 4, where the tilde–hatted PDFs are calculated via the proposed method. The required augmenting sample sizes are $N_{\text{aug}} = 3, 40, 0, 77, 87$ corresponding to Case 1 to Case 5 in order. The GF-discrepancies of the first 5 cases are 0.0039 (0.0048), 0.0092 (0.0497), 0.0048 (0.0056), 0.0048 (0.1245), 0.0050 (0.2494), where the value outside of the bracket is by aCOM while the one in the bracket stands for the result by direct COM.

Algorithm 1 The proposed approach for hybrid uncertainty propagation.

Require:
The prior and new PDFs of Θ in order, $p_{\Theta}^{(1)}(\theta)$ and $p_{\Theta}^{(2)}(\theta)$
Number of partitions of assigned-probability space, $N \in \mathbb{N}^+$
Order of B-spline chaos and number of B-spline basis functions, $p \in \mathbb{N}^+$ and $n \in \mathbb{N}^+$

Ensure:
The PDFs of X with respect to $p_{\Theta}^{(1)}(\theta)$ and $p_{\Theta}^{(2)}(\theta)$ in order, $p_X^{(1)}(x)$ and $p_X^{(2)}(x)$

▽ *Generate the initial point set via partition of assigned-probability space*
$\mathcal{M}^{(1)} \leftarrow \{\theta_q^{(1)}; P_q^{(1)}\}_{q=1}^{N} \sim p_{\Theta}^{(1)}(\theta)$ ▷ Appendix A
▽ *Generate the augmenting point set via aCOM*:
Estimate the augmenting sample size, $N_{\text{aug}} \leftarrow \left\lceil \left(\pi_a^{(2)} - \pi_a^{(1)}\right) \cdot N \right\rceil$ ▷ by Eq. (17)
if $N_{\text{aug}} = 0$ **then**
  $\{\theta_q^{(2)}\}_{q=1}^{N} \leftarrow \{\theta_q^{(1)}\}_{q=1}^{N}$
else
  Construct the augmenting PDF, $p_{\Theta}^{(\text{aug})}(\theta)$ ▷ by Eq. (18)
  Generate augmenting points, $\{\theta_q^{(\text{aug})}\}_{q=1}^{N_{\text{aug}}} \leftarrow p_{\Theta}^{(\text{aug})}(\theta)$ ▷ by inverse-transform method
  $\{\theta_q^{(2)}\}_{q=1}^{N+N_{\text{aug}}} \leftarrow \{\theta_q^{(1)}\}_{q=1}^{N} \cup \{\theta_q^{(\text{aug})}\}_{q=1}^{N_{\text{aug}}}$ ▷ by Eq. (19)
end if
$\mathcal{M}^{(2)} \leftarrow \{\theta_q^{(2)}; P_q^{(2)}\}_{q=1}^{N+N_{\text{aug}}} \sim p_{\Theta}^{(2)}(\theta)$ ▷ $P_q^{(2)}$ by Eq. (20)
▽ *Deterministic analysis*:
for $q = 1, \cdots, N + N_{\text{aug}}$ **do**
  $x_q^{(2)} \leftarrow g\left(\theta_q^{(2)}\right)$ ▷ by Eq. (1)
  $x_q^{(1)} \leftarrow x_q^{(2)}$ ▷ for $q = 1, \cdots, N$
end for
▽ *Construction of B-spline chaos via partition of assigned-probability space*
For $p_{\Theta}^{(1)}(\theta)$, solve $\mathbf{B}^{(1)}\mathbf{b}^{(1)} = \mathbf{x}^{(1)}$ using $\{\theta_q^{(1)}, x_q^{(1)}, P_q^{(1)}\}_{q=1}^{N}$ ▷ by Eqs. (22) and (23)
For $p_{\Theta}^{(2)}(\theta)$, solve $\mathbf{B}^{(2)}\mathbf{b}^{(2)} = \mathbf{x}^{(2)}$ using $\{\theta_q^{(2)}, x_q^{(2)}, P_q^{(2)}\}_{q=1}^{N+N_{\text{aug}}}$ ▷ by Eqs. (24) and (25)
▽ *Estimate PDFs of X via B-spline chaos and MCS-KDE*:
$p_X^{(1)}(x)$ via MCS-KDE ▷ using 10^6 MCS samples from B-spline chaos constructed by $\mathbf{b}^{(1)}$
$p_X^{(2)}(x)$ via MCS-KDE ▷ using 10^6 MCS samples from B-spline chaos constructed by $\mathbf{b}^{(2)}$

It can be seen that the new point set via aCOM can have a smaller GF-discrepancy than the one by COM.

For Case 1 in Fig. 4(b), since a very small shift in mean value is applied, it is only required to augment 3 additional samples to reconstruct $p_X^{(2)}(x)$. Interestingly, for Case 3 in Fig. 4(d) that shows a large change in standard deviation, no extra points are needed via the proposed method. This is reasonable because the support of $p_{\Theta}^{(1)}(\theta)$ completely covers the region of $p_{\Theta}^{(2)}(\theta)$ in a numerical sense. Consequently, both accuracy and efficiency are well achieved via the proposed method for the first 5 cases.

The last 5 cases of hybrid uncertainty propagation take into account three typical distributions, i.e., Normal distribution (with an infinite support), Beta distribution (with a bounded support), and Lognormal distribution (with a semi-infinite support):

- Case 6: Bounded to Infinite – $p_{\Theta}^{(1)}(\theta) = \mathcal{B}(1.275, 2.975)$ to $p_{\Theta}^{(2)}(\theta) = \mathcal{N}(0.3, 0.2)$,
- Case 7: Bounded to Semi-infinite – $p_{\Theta}^{(1)}(\theta) = \mathcal{B}(1.275, 2.975)$ to $p_{\Theta}^{(2)}(\theta) = \mathcal{LN}(-1.388, 0.606)$,
- Case 8: Semi-infinite to Bounded – $p_{\Theta}^{(1)}(\theta) = \mathcal{LN}(-1.388, 0.606)$ to $p_{\Theta}^{(2)}(\theta) = \mathcal{B}(1.275, 2.975)$,

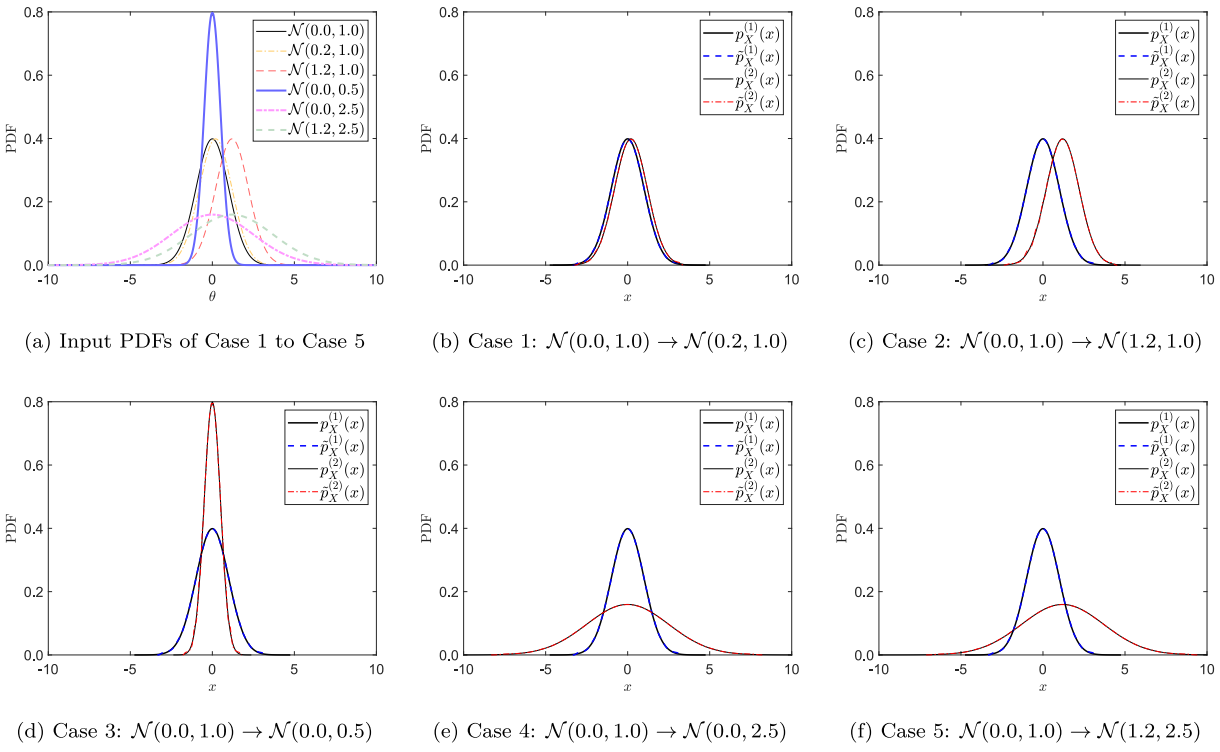

(a) Input PDFs of Case 1 to Case 5 (b) Case 1: $\mathcal{N}(0.0,1.0) \to \mathcal{N}(0.2,1.0)$ (c) Case 2: $\mathcal{N}(0.0,1.0) \to \mathcal{N}(1.2,1.0)$

(d) Case 3: $\mathcal{N}(0.0,1.0) \to \mathcal{N}(0.0,0.5)$ (e) Case 4: $\mathcal{N}(0.0,1.0) \to \mathcal{N}(0.0,2.5)$ (f) Case 5: $\mathcal{N}(0.0,1.0) \to \mathcal{N}(1.2,2.5)$

Fig. 4. Verification of the proposed method for approximation of basic random variables (Case 1 to Case 5).

- Case 9: Semi-infinite to Infinite – $p_\Theta^{(1)}(\theta) = \mathcal{LN}(-1.388, 0.606)$ to $p_\Theta^{(2)}(\theta) = \mathcal{N}(0.3, 0.2)$,
- Case 10: Infinite to Semi-infinite – $p_\Theta^{(1)}(\theta) = \mathcal{N}(0.3, 0.2)$ to $p_\Theta^{(2)}(\theta) = \mathcal{LN}(-1.388, 0.606)$,

where $\mathcal{B}(a,b)$ stands for the Beta distribution whose PDF is $\frac{\theta^{a-1}(1-\theta)^{b-1}}{B(a,b)}$ where $B(a,b) = \frac{\Gamma(a)\Gamma(b)}{\Gamma(a+b)}$ and $\Gamma(\cdot)$ is the Gamma function; $\mathcal{LN}(a,b)$ is the Lognormal distribution, i.e., $\frac{1}{\theta b\sqrt{2\pi}} \exp\left(-\frac{(\ln\theta - a)^2}{2b^2}\right)$. It is emphasized that the three distributions have the same mean value 0.3 and the standard deviation 0.2, resulting in an coefficient of variation of 66.7% that is practical for most real engineering problems.

The results of the last 5 cases are shown in Fig. 5, where a consistent accuracy is achieved from Figs. 5(b) to 5(f), but the required number of augmenting samples is different, i.e., from Case 6 to Case 10 in order that $N_{\text{aug}} = 14, 4, 21, 22, 5$. The GF-discrepancies of the last 5 cases are 0.0034 (0.0674), 0.0058 (0.0176), 0.0045 (0.0649), 0.0048 (0.0992), 0.0053 (0.0191), which again shows a small GF-discrepancy via aCOM.

Note that though Case 7 and Case 8 both consider the same Beta and Lognormal distributions, the required augmenting samples are quite different, i.e., $N_{\text{aug}} = 4$ for Case 7 while $N_{\text{aug}} = 21$ for Case 8. One can see a similar result for Case 9 and Case 10 that consider the same Lognormal and Normal distributions but $N_{\text{aug}} = 22$ for Case 9 and $N_{\text{aug}} = 5$ for Case 10. The above results indicate that *information asymmetry* may exist in the propagation of hybrid uncertainty.

4.2.2. Ishigami function

The second specific example takes the classical Ishigami function in a simplified univariate form [28]:

$$X = \sin(\Theta) + 7\sin^2(\Theta) + 0.1\Theta^4 \sin(\Theta), \tag{26}$$

where Θ is a uniform random variable whose PDF is taken from Fig. 6(a).

The results for $p_\Theta^{(1)}(\theta) = \mathcal{U}(-\pi, \pi)$ to $p_\Theta^{(2)}(\theta) = \mathcal{U}(-\pi/2, \pi/2)$ are shown in Fig. 6(b), where $p_X(x)$ is calculated via MCS. Since the support of $p_\Theta^{(2)}(\theta)$ is fully covered by the one of $p_\Theta^{(1)}(\theta)$, no augmenting samples are needed. However, for the case that $p_\Theta^{(1)}(\theta) = \mathcal{U}(-\pi/2, \pi/2)$ to $p_\Theta^{(2)}(\theta) = \mathcal{U}(-\pi/2, \pi)$ in Fig. 6(c), a number of 67 augmenting samples are required. Although the studied Ishigami function exhibits a strong nonlinearity, the accuracy of results via the proposed method can still be satisfied.

4.2.3. Series system with four branches and two independent or dependent random variables

For the case of high-dimensional inputs, one direct way to enhance the proposed method is to first introduce a specific dimension reduction technique to decrease the dimension of high-dimensional inputs. For instance, consider a series system with four branches and two input random variables [29,30], which reads:

$$X = \min \begin{cases} X_1 = 3.0 + 0.1(\Theta_1 - \Theta_2)^2 + (\Theta_2 - \Theta_1)/\sqrt{2}, \\ X_2 = 3.0 + 0.1(\Theta_1 - \Theta_2)^2 + (\Theta_1 - \Theta_2)/\sqrt{2}, \\ X_3 = (\Theta_1 - \Theta_2) + 3.0\sqrt{2}, \\ X_4 = (\Theta_2 - \Theta_1) + 3.0\sqrt{2}, \end{cases} \tag{27}$$

where Θ_1 and Θ_2 are independent uniform random variables for the independent case, and Θ_1 and Θ_2 are multivariate normal variables for the dependent case. The epistemic uncertainty is considered as follows:

(1) Independent case: From $\theta_1 \times \theta_2 = [-2, 0] \times [0, 2]$ to $\theta_1 \times \theta_2 = [-1, 0] \times [0, 1]$;

(2) Dependent case: From $(\boldsymbol{\mu}_1, \mathbf{D}_1) = \left(\begin{bmatrix}-0.5\\0.1\end{bmatrix}, \begin{bmatrix}1/3 & 0.25\\0.25 & 1/3\end{bmatrix}\right)$ to $(\boldsymbol{\mu}_2, \mathbf{D}_2) = \left(\begin{bmatrix}-0.5\\0.5\end{bmatrix}, \begin{bmatrix}1/12 & 0.04\\0.04 & 1/12\end{bmatrix}\right)$, where $(\boldsymbol{\mu}, \mathbf{D})$ stands for the mean vector $\boldsymbol{\mu}$ and covariance matrix $\mathbf{D}$ of $\boldsymbol{\Theta} = (\Theta_1, \Theta_2)^\top$, respectively.

The active subspace method (ASM) [27] is first utilized for the dimension reduction (see Appendix C), which results in $\hat{\theta} = \hat{\mathbf{W}}^\top \boldsymbol{\theta} \in \mathbb{R}^1$, where $\hat{\mathbf{W}} = [-1/\sqrt{2}, 1/\sqrt{2}]^\top$. Then, the B-spline chaos is constructed in the $\hat{\theta} - x$ space. The results of dimension reduction are shown in Figs. 7(a) and 7(b) for the independent case, and in Figs. 7(c) and 7(d) for the dependent case. The PDFs and CDFs of X for the hybrid

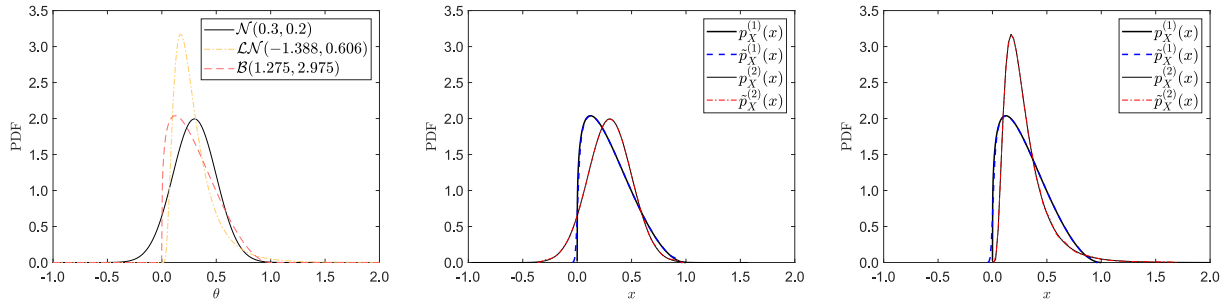

(a) Input PDFs of Case 6 to Case 10 (b) Case 6: Beta to Normal (c) Case 7: Beta to Lognormal

(d) Case 8: Lognormal to Beta (e) Case 9: Lognormal to Normal (f) Case 10: Normal to Lognormal

Fig. 5. Verification of the proposed method for approximation of basic random variables (Case 6 to Case 10).

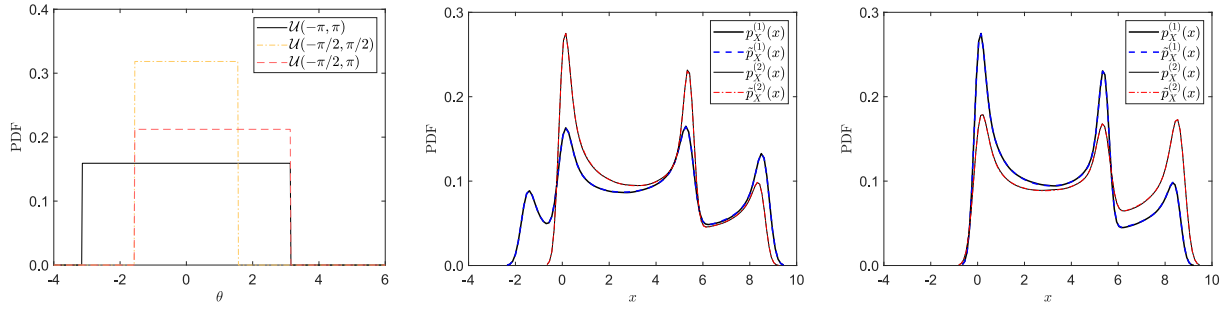

(a) Input PDFs (b) From $\mathcal{U}(-\pi, \pi)$ to $\mathcal{U}(-\pi/2, \pi/2)$ (c) From $\mathcal{U}(-\pi/2, \pi/2)$ to $\mathcal{U}(-\pi/2, \pi)$

Fig. 6. Verification of the proposed method for Ishigami function.

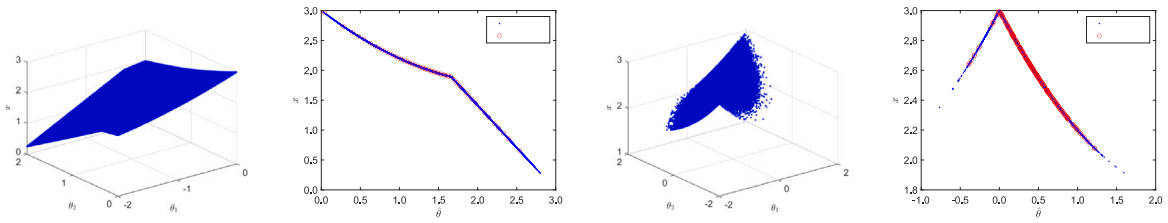

(a) $\boldsymbol{\theta}$-x space (Independent case) (b) $\hat{\theta}$-x space (Independent case) (c) $\boldsymbol{\theta}$-x space (Dependent case) (d) $\hat{\theta}$-x space (Dependent case)

Fig. 7. One-dimensional active subspace of the series system with four branches.

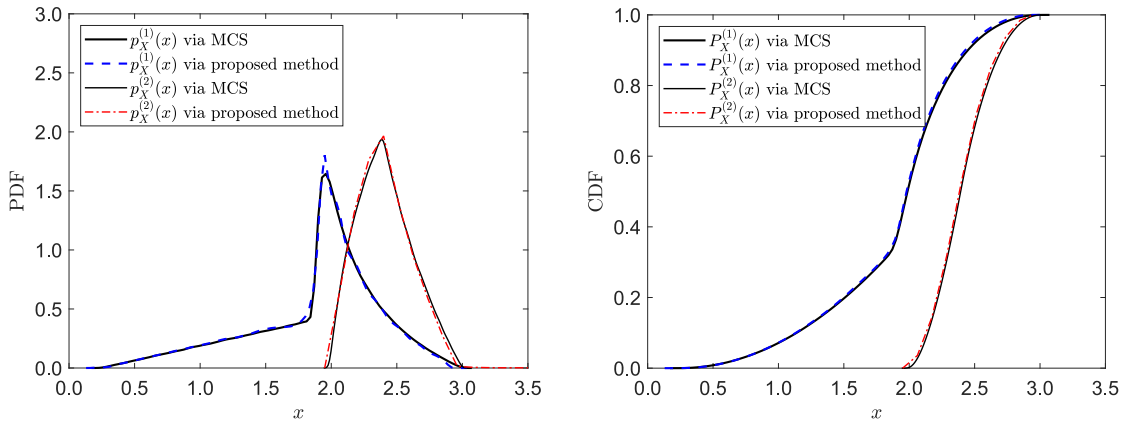

(a) PDFs of X (b) CDFs of X

Fig. 8. Verification of the proposed method for the series system with four branches (independent case).

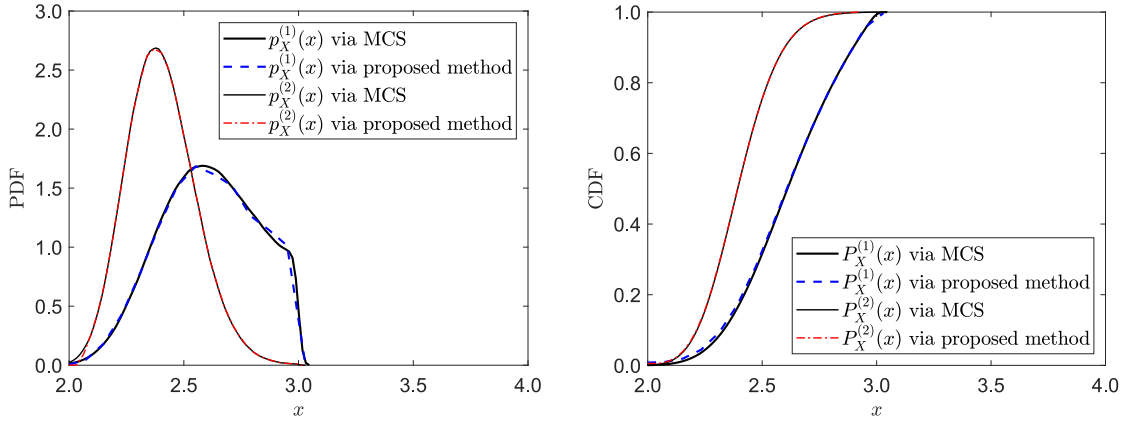

(a) PDFs of X (b) CDFs of X

Fig. 9. Verification of the proposed method for the series system with four branches (dependent case).

uncertainty propagation are presented in Fig. 8 for the independent case and in Fig. 9 for the dependent case. From the results of both cases, it can be seen that the proposed method could still provide relatively good accuracy.

A more practical application with higher-dimensional inputs is illustrated in the following Example 4, where the first step is to detect a one-dimensional active subspace as the same as this example. However, it should be emphasized that not all problems may exist such a one-dimensional active subspace.

4.2.4. Special non-smooth function

The last example is adopted from [16] to illustrate to the reader in which cases one should carefully consider the potential deterioration of accuracy of the proposed method.

For illustration, consider a one-dimensional function that

$$X = \exp(-3|\Theta|), \tag{28}$$

where the PDF of Θ is changed from $\mathcal{U}(-1.0, 0.0)$ (Problem 1) to $\mathcal{U}(-0.5, 0.5)$ (Problem 2). From Fig. 10(a), one can see that $x = g(\theta)$ for $\theta \in [-1.0, 0.0]$ is of class C^1, while it is of C^0 in the region $\theta \in [-0.5, 0.5]$.

Let us first consider Problem 1 as a *perfect* problem, namely, the information that g for $\theta \in [-1.0, 0.0]$ is of C^1 is known based on the expertness of analyst. Therefore, one may be confident that it is accurate enough to set $N = 20$, $p = 2$ and $n = 10$ to estimate $p_X^{(1)}(x)$ via the proposed method, as shown in Fig. 10(b).

Now it comes to Problem 2, which is regarded as a *gray-box* problem, viz., g for $\theta \in [-0.5, 0.0]$ is known to be of C^1, but we have no prior knowledge that g is of C^0 for $\theta \in [-0.5, 0.5]$. Then, the proposed method is employed again, and the convergence analysis is conducted by increasing parameters in B-spline chaos, e.g., n, the number of B-spline basis functions. Noticing that for Problem 1 we set $N = 20$, which means the maximum value of n is 20, otherwise numerical singularity would occur. The convergence analysis gives the final estimated $\tilde{p}_X^{(2)}(x)$ as shown in Figs. 10(b) and 10(c) with respect to $n = 10$ and $n = 20$. Compared with the exact $p_X^{(2)}(x)$, it is obvious that one needs to keep enlarging n. Nonetheless, misled by the parameters determined for Problem 1, we have limited ourselves to $n = 20$ for solving Problem 2.

In short, we want to emphasize that the proposed method with parameters $N = 200$, $p = 10$ and $n = 30$ determined for solving all other examples in this work, is not a one-size-fits-all solution. For real engineering practices involved with hybrid uncertainties, the significance of the analyst should also be highlighted [26].

4.3. Remarks on efficiency, limitations, and potential improvements of the proposed method

Efficiency. The efficiency of the proposed method can be more pronounced if Θ (due to epistemic uncertainty) may obey more than two PDFs defined by $p_\Theta^{(1)}(\theta), \ldots, p_\Theta^{(M)}(\theta)$, where $M \in \mathbb{N} \geq 3$. For the sake of simplicity, assume for each certain $p_\Theta(\theta)$ a total number of N model evaluations are required and let the time cost for one

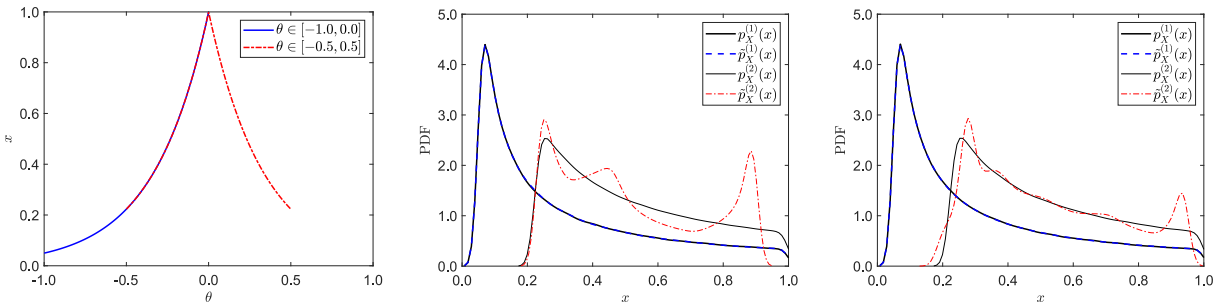

(a) $x = g(\theta)$ (b) $p = 2$ and $n = 10$ (c) $p = 2$ and $n = 20$

Fig. 10. The situation that the accuracy of the proposed method may deteriorate.

deterministic analysis be t_0. Then, in general, the total computational time for dealing with such hybrid uncertainty propagation issue is $T_{\text{UQ}} = N \times M \times t_0 = (N + \sum_{i=2}^{M} N) \times t_0$. However, from the preceding numerical illustrations, the total time cost for the proposed method becomes $T_{\text{UQ}}^{\text{aCOM}} = (N + \sum_{i=2}^{M} N_{\text{aug}}^{(i)}) \times t_0 + (M - 1) \times t_{\text{aCOM}}$, where $0 \le N_{\text{aug}}^{(i)} \le N$ is the augmenting sample size with respect to $p_{\Theta}^{(i)}(\theta)$, and t_{aCOM} is the time cost for implementing the aCOM. Note that t_{aCOM} is extremely smaller than t_0 – the former takes only seconds while the latter may range from minutes to hours or even days, depending on the complexity of the engineering model. Therefore, we have

$$\frac{T_{\text{UQ}}^{\text{aCOM}}}{T_{\text{UQ}}} = \frac{(N + \sum_{i=2}^{M} N_{\text{aug}}^{(i)}) \times t_0 + (M-1) \times t_{\text{aCOM}}}{(N + \sum_{i=2}^{M} N) \times t_0} \approx \frac{N + \sum_{i=2}^{M} N_{\text{aug}}^{(i)}}{N + \sum_{i=2}^{M} N} \in [1/M, 1], \tag{29}$$

which means the computational cost via the proposed method can be reduced by a maximum factor of M.

Limitations. At present, our proposed method presents high accuracy as well as efficiency for the issue of hybrid uncertainty propagation that involves only one input random variable. This limitation is due to the introduced B-spline chaos in [15] that only adopts one-dimensional B-spline basis functions. Similar to other framework studies, although this limitation is relatively strict, it is meaningful to understanding the basic idea of the proposed framework for hybrid uncertainty propagation based on B-spline chaos and aCOM, especially for most engineers who are not familiar with these two advancing UQ techniques.

Potential improvements. Any improvements to the B-spline chaos and aCOM may contribute to the proposed method. For instance, for high-dimensional cases, multivariate B-spline chaos [16] could be an alternative, but the computational cost may increase exponentially due to the tensor-product structure. This issue could be alleviated by B-splines on sparse grids [31] or spline dimensional decomposition [32]. Besides, multivariate COM [4] has been investigated in corporation with probability density evolution method, but currently it is only suitable for cases of small epistemic uncertainty. Moreover, adopting dimension reduction techniques, such as active subspace method [27] (as illustrated above), probabilistic learning on manifolds [33], etc., could possibly improve the proposed method as well. But certainly, introducing an extra module for dimension reduction may, more or less, increase the computational cost for hybrid uncertainty propagation.

5. Numerical examples

5.1. Example 1: Three classical oscillators

This example studies three classical oscillators that are commonly used as benchmarks to uncertainty propagation analysis [13,22,34–36], including: (1) a linear undamped equation, (2) a Van der Pol equation, and (3) a Riccati equation, respectively.

5.1.1. Linear undamped equation

The motion of the first oscillator is governed by the following linear undamped equation written by

$$\ddot{x} + \theta^2 x = 0, \ x(0) = 1, \ \dot{x}(0) = 0, \tag{30}$$

where $\ddot{x}$, $\dot{x}$, and x stand for the acceleration, velocity, and displacement in terms of the time, respectively.

Let θ be a uniform random variable whose PDF is defined by $p_{\Theta}(\theta) = \frac{1}{b-a}$ for $\theta \in [a, b]$, otherwise $p_{\Theta}(\theta) = 0$. Knowing the formal solution of Eq. (30) that

$$x = x_0 \cos(\theta t), \tag{31}$$

the analytical PDF of X can be derived by [37]

$$p_X(x,t) = \frac{t^{-1}}{\sqrt{x_0^2 - x^2}} \sum_{\ell=0}^{\infty} p_{\Theta}\left(\theta = \frac{2\ell\pi + 2\pi}{t} - \frac{1}{t}\cos^{-1}\left(\frac{x}{x_0}\right)\right) + p_{\Theta}\left(\theta = \frac{2\ell\pi}{t} + \frac{1}{t}\cos^{-1}\left(\frac{x}{x_0}\right)\right) \tag{32}$$

for $|x| \le |x_0|$, otherwise $p_X(x,t) = 0$.

Let $p_{\Theta}^{(1)}(\theta) = \mathcal{U}(5/4\pi, 7/4\pi)$ and $p_{\Theta}^{(2)}(\theta) = \mathcal{U}(\pi, 2\pi)$ be the input PDFs of Θ due to the epistemic uncertainty. With the proposed method, the probabilistic information of Eq. (30) is depicted in Fig. 11. The evolution of PDFs of X at $t = 1.0$ s and $t = 2.4$ s are shown in Figs. 11(a) and 11(b), respectively. One can see that the PDF of X is varying with time, and is remarkably different from the uniform distribution. It is noted that the calculated PDF of X will be smoothed via KDE for those jump points in the realizations of X as illustrated in Fig. 11(c), which is the main source of error that leads to a slight discrepancy in Fig. 11(b). Except for this, the proposed method accords perfectly with the analytical solution.

5.1.2. Van der Pol equation

Consider the Van der Pol equation written by

$$\ddot{x} + \theta\dot{x}x^2 + x = 0, \ x(0) = 1, \ \dot{x}(0) = 0. \tag{33}$$

We assume that the damping coefficient θ in Eq. (33) has a small value (e.g., $0 < \theta < 1$) and follows the Beta distribution $\mathcal{B}(a, b)$. Specifically, let $p_{\Theta}^{(1)}(\theta) = \mathcal{B}(3,3)$ and $p_{\Theta}^{(2)}(\theta) = \mathcal{B}(2,6)$ as shown in Fig. 12(a). By doing this, an approximate solution of Eq. (33) can be given by [38]

$$x \approx \cos t - \frac{1}{8}t\theta\cos^3 t + \frac{1}{8}\theta\sin^3 t, \tag{34}$$

and its analytical PDF can be derived by [13]

$$p_X(x,t;a,b) = p_{\Theta}\left(\theta = \frac{8(x - \cos t)}{\sin^3 t - t\cos^3 t}; a, b\right) \Big/ \left|\frac{1}{8}\sin^3 t - \frac{1}{8}t\cos^3 t\right|. \tag{35}$$

The results are shown in Fig. 12(b) for the time instant $t = 3$ s and Fig. 12(c) for $t = 6$ s. It is seen that due to the epistemic uncertainty of Θ, there is a distinct variation in the PDF configuration of X at various time instants. Besides, according to the error of PDF

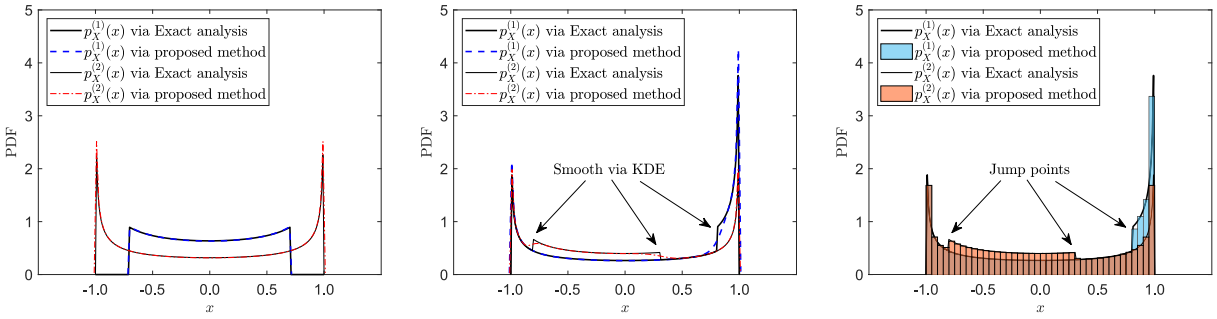

(a) PDFs of X at $t = 1.0$ sec (b) PDFs of X at $t = 2.4$ sec (c) Histograms of X at $t = 2.4$ sec

Fig. 11. PDF evolution of linear undamped equation (Example 1).

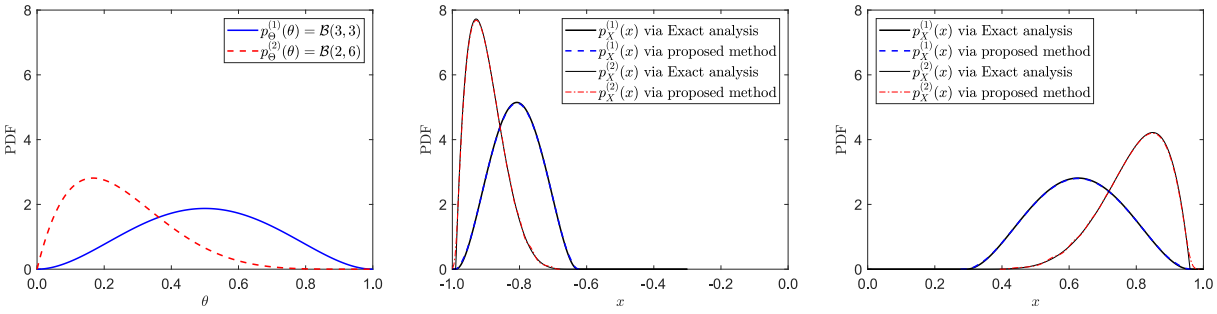

(a) Input PDFs of Θ (b) PDFs of X at $t = 3$ sec (c) PDFs of X at $t = 6$ sec

Fig. 12. PDF evolution of Van der Pol equation (Example 1).

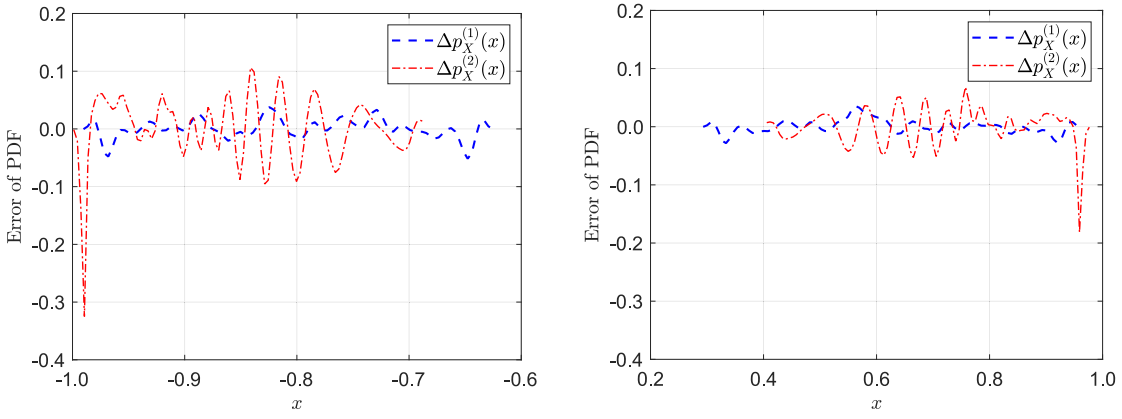

(a) Error of PDFs of X at $t = 3$ sec (b) Error of PDFs of X at $t = 6$ sec

Fig. 13. Error of PDF evolution of Van der Pol equation (Example 1).

of X shown in Fig. 13, i.e., the difference between the exact PDF and the estimated PDF, it can be seen that the proposed method exhibits well accuracy and good efficiency that only requires to augment 50 additional samples.

5.1.3. Riccati equation

Consider the following Riccati equation:

$$\dot{x} + \theta x^2 - x = 0, \quad x(0) = x_0, \tag{36}$$

and assume that θ is a random variable following the standard Normal distribution $p_\Theta^{(1)}(\theta) = \mathcal{N}(0,1)$ and the standard Lognormal distribution $p_\Theta^{(2)}(\theta) = \mathcal{LN}(0,1)$. Let $x_0 = 0.1$ be a deterministic initial condition, thus the initial velocity becomes a random variable $x_0 - \Theta x_0^2$.

With the analytical solution of Eq. (36) given by [38]

$$x(t) = \frac{e^t x_0}{\theta(e^t - 1)x_0 + 1}, \tag{37}$$

the PDFs of X in terms of $p_\Theta^{(1)}(\theta)$ and $p_\Theta^{(2)}(\theta)$ can be derived as

$$p_X^{(1)}(x) = \frac{e^t}{\sqrt{2\pi x^2(e^t - 1)}} \exp\left(-\frac{1}{2}\left\{\frac{e^t x_0 - x}{x(e^t x_0 - x_0)}\right\}^2\right) \tag{38}$$

and

$$p_X^{(2)}(x) = \frac{e^t x_0}{\sqrt{2\pi x(e^t x_0 - x)}} \exp\left(-\frac{1}{2}\left\{\ln\frac{e^t x_0 - x}{x(e^t x_0 - x_0)}\right\}^2\right), \tag{39}$$

respectively.

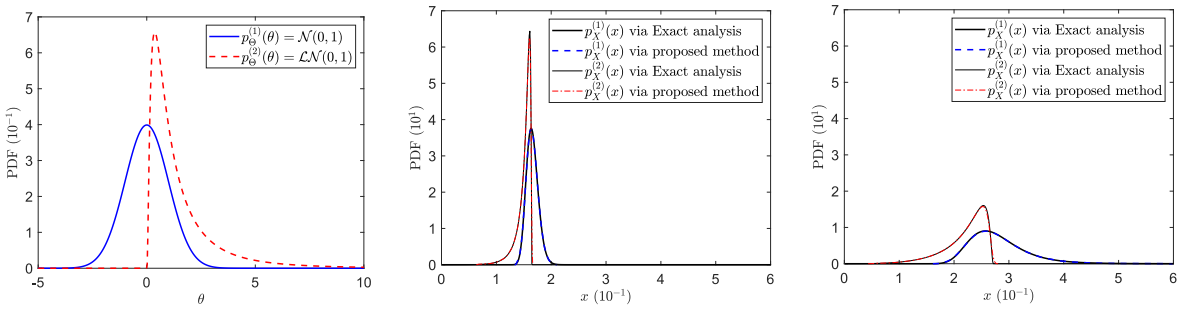

(a) Input PDFs of Θ (b) PDFs of X at $t = 0.5$ sec (c) PDFs of X at $t = 1.0$ sec

Fig. 14. PDF evolution of Riccati equation (Example 1).

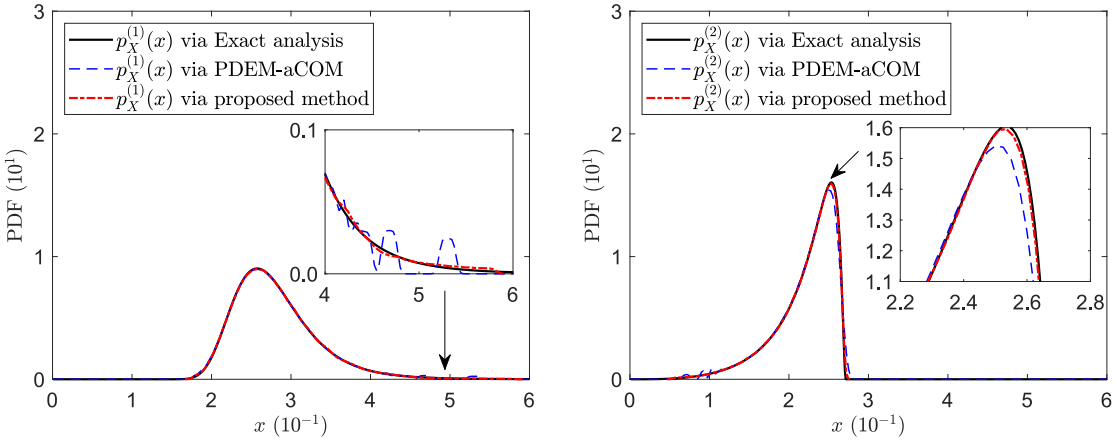

(a) PDFs of X at $t = 1.0$ sec in terms of $p_\Theta^{(1)}(\theta)$ (b) PDFs of X at $t = 1.0$ sec in terms of $p_\Theta^{(2)}(\theta)$

Fig. 15. PDF evolution of Riccati equation via the proposed method and PDEM-aCOM (Example 1).

The PDF results of X are shown in Fig. 14(b) for $t = 0.5$ s and Fig. 14(c) for $t = 1.0$ s, from which it can be observed that the PDF of X exhibits a rapid fall with increasing time. In addition, the nonlinearity of the Riccati equation allows for the non-Gaussian nature of the PDF of X, even when the input PDF follows a Gaussian distribution. Once more, the accuracy of the proposed method is granted with only 46 augmenting samples. Fig. 15 compares the accuracy of the proposed method and the probability density evolution method (PDEM) integrated with the aCOM (shorted as "PDEM-aCOM" [13]). Although the results via the two methods, on the whole, are both consistent with the analytical solutions, the proposed method has higher accuracy on local PDFs.

5.2. Example 2: A jet engine turbine blade model

Fig. 16(a) illustrates a finite element model of a turbine blade in a jet engine [13], utilizing a tetrahedral mesh. The turbine blade consists of a radial arrangement of blades, commonly composed of nickel alloys such as NI-MONIC 90. These blades operate in environments characterized by pressure loading and elevated temperatures. The computational cost associated with this model is notably higher compared to Example 1, however comparatively lower than that of the subsequent Example 3. Therefore, we take the MCS results of 10 000 model evaluations as reference solutions.

A total of six significant model parameters are considered in previous UQ studies [39,40], including the Young's modulus E, coefficient of thermal expansion α, Poisson's ratio ν, thermal conductivity κ, and two external loads, i.e., pressure loads P_{pre} and P_{suc} on the pressure and suction sides of the blade, respectively. According to the sensitivity analysis in [39,40], the coefficient of thermal expansion is the dominant parameter that is most sensitive to the maximum deformation (denoted by x) of the turbine blade. For this reason, consider $\alpha = \Theta$ be a random variable following $p_\Theta^{(1)}(\theta) = \mathcal{N}(12.7, 1.27)$ and $p_\Theta^{(2)}(\theta) = \mathcal{N}(10.0, 1.50)$ (unit in 10^{-6} 1/K), as shown in Fig. 16(b), and the values of other parameters are taken as $E = 227$ GPa, $\nu = 0.27$, $\kappa = 11.5$ W/m/K, $P_{\text{pre}} = 800$ kPa, and $P_{\text{suc}} = 600$ kPa.

The PDFs of X are shown in Fig. 16(c), where the required number of augmenting samples is 107. Again, a good agreement is achieved by the proposed method compared to the MCS solutions. The accuracy of the proposed method can also be observed in Fig. 17, from which the estimated failure probability can reach an accuracy of $\mathcal{O}(10^{-3})$. Overall, the leftward PDF of X indicates that as the coefficient of thermal expansion decreases, the maximum deformation will be reduced as well. Interestingly, although $p_\Theta^{(2)}(\theta)$ has a larger standard deviation than $p_\Theta^{(1)}(\theta)$, the PDFs of X present almost the same standard deviation. This result shows that although the coefficient of thermal expansion is sensitive to the maximum deformation, the standard deviation of the coefficient of thermal expansion may not be the same, which is consistent with the study in [40].

5.3. Example 3: A wind turbine tower model of two dry-joined circular ring segments

This example studies the uncertainty of interface friction coefficient $\mu = \Theta$ on the torsion capacity $M_{\text{T}} = X$ of a wind turbine tower model, which is simplified by two dry-joined circular ring segments as shown in Fig. 18(a) The geometric information, external loads, and material properties of concrete in the model are referred to [41], as listed in

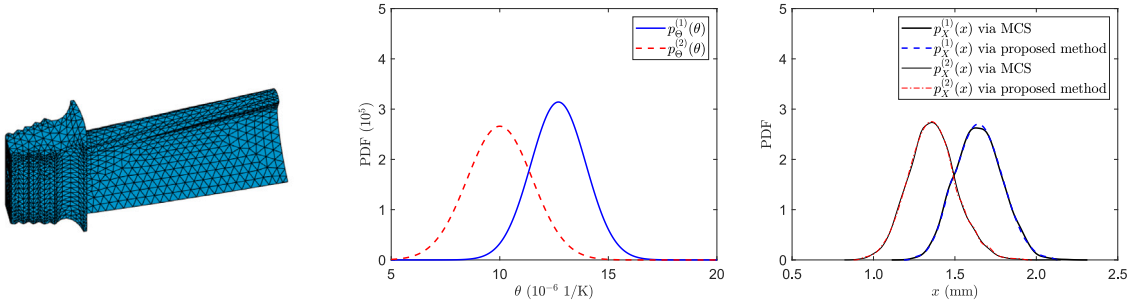

(a) Finite element model (b) Input PDFs (c) PDFs of the maximum deformation

Fig. 16. Hybrid uncertainty propagation of a jet engine turbine blade model (Example 2).

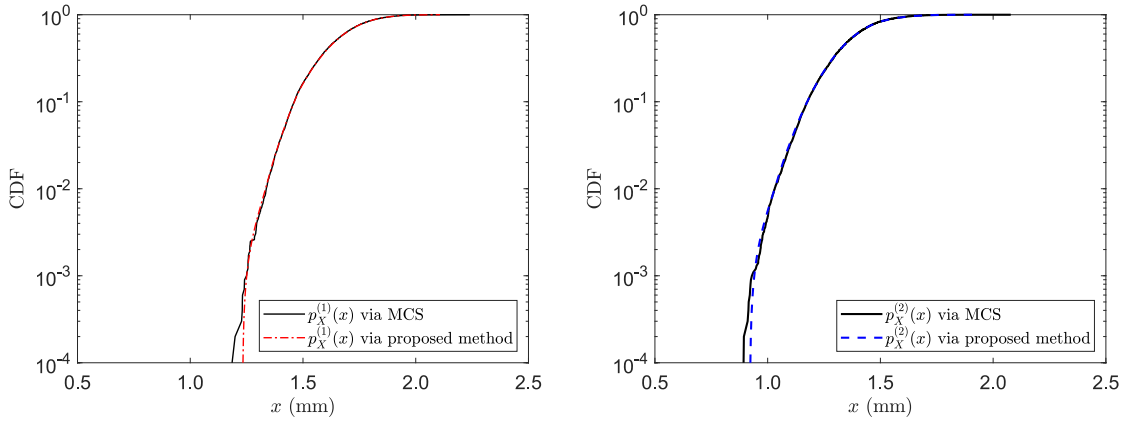

(a) CDF of X in terms of $p_\Theta^{(1)}(\theta)$ (b) CDF of X in terms of $p_\Theta^{(2)}(\theta)$

Fig. 17. CDFs of X in terms of $p_\Theta^{(1)}(\theta)$ and $p_\Theta^{(2)}(\theta)$ (Example 2).

Table 1
Model parameters in Example 3.

Geometric information			External load	
Height	Outer radius	Thickness	Axial force	Bending moment
0.5 m × 2	0.3 m	0.05 m	300.4 kN	45.5 kN m
Material property				
Compressive strength	Modulus of elasticity	Density	Poisson's ratio	Friction coefficient
83 MPa	37 000 MPa	2400 kg/m^3	0.2	Θ

Table 1. The friction coefficient is considered to be a random variable with PDFs $p_\Theta^{(1)}(\theta) = \mathcal{U}(0.3, 0.8)$ and $p_\Theta^{(2)}(\theta) = \mathcal{U}(0.4, 0.7)$. Note that the two PDFs have the same mean value of 0.55 that is according to the model experiment in [41].

The model is made of plain concrete materials and the influence of material nonlinearity is not considered, but the contact nonlinearity and the geometric nonlinearity are both taken into account. As a result, a total of 45 696 hexahedral elements with 60 113 nodes are developed (Fig. 18(b)), amounting to 175 854 degrees of freedom. Loads are applied sequentially in the order of axial force, bending moment, and torsion. The first two are applied by force method, while the last is applied via displacement method. The torsion capacity is determined by the stable torsion value of the torque–angle curve as illustrated in Fig. 19(a).

The PDFs of the torsion capacity are shown in Fig. 19(b), from which it can be seen that a significant reduction in the distribution region of torsion capacity as the distribution of friction coefficient becomes narrower. Note that this result is computed via the proposed method with no additional model evaluations, since the region of $p_\Theta^{(1)}(\theta)$ fully covers the one of $p_\Theta^{(2)}(\theta)$.

5.4. Example 4: Golinski's speed reducer design issue

The last example tests the well-known standard problem in the NASA Langley MDO Test Suite [42]. The system response is formulated mathematically by

$$\begin{aligned} X &= 0.7854\Theta_1\Theta_2^2(3.3333\theta_3^2 + 14.9334\theta_3 - 43.0934) \\ &\quad - 1.5079\Theta_1(\Theta_6^2 + \Theta_7^2) + 7.477(\Theta_6^3 + \Theta_7^3) + 0.7854(\Theta_4\Theta_6^2 + \Theta_5\Theta_7^2), \end{aligned} \tag{40}$$

where θ_3 is a deterministic integer in $[17, 28]$, while other parameters are taken as independent and uniform random variables. The hybrid uncertainty propagation is considered from Problem 1 as per [42] to Problem 2 as follows:

(1) Problem 1: $\theta_1 \in [2.6, 3.6]$, $\theta_2 \in [0.7, 0.8]$, $\theta_4 \in [7.3, 8.3]$, $\theta_5 \in [7.3, 8.3]$, $\theta_6 \in [2.9, 3.9]$, $\theta_7 \in [5.0, 5.5]$.

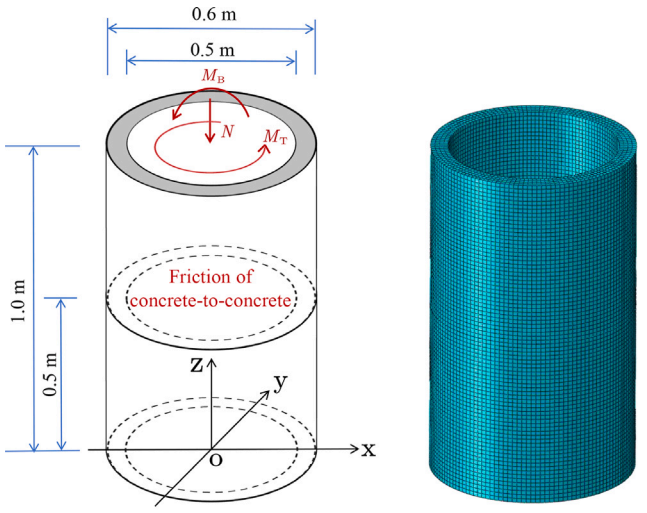

(a) Model information (b) Mesh model

Fig. 18. Model of a wind turbine tower simplified by two dry-joined circular ring segments (Example 3).

(2) Problem 2: $\theta_1 \in [2.8, 3.4]$, $\theta_2 \in [0.7, 0.8]$, $\theta_4 \in [7.6, 8.0]$, $\theta_5 \in [7.6, 8.0]$, $\theta_6 \in [2.9, 3.9]$, $\theta_7 \in [5.0, 5.5]$.

The active subspace method in Appendix C is first applied to reduce the original input space of $\boldsymbol{\theta} \in \mathbb{R}^6$ into the active input space of $\hat{\theta} \in \mathbb{R}^1$. Then, the proposed method is adopted for the hybrid uncertainty propagation problem. Figs. 20(a) and 20(b) show the results of cross-validation by using $N = 500$ samples, and the CDFs of X via the proposed method with $p = 1$ and $n = 15$ for Problem 1 ($P_X^{(1)}(x)$) and Problem 2 ($P_X^{(2)}(x)$) are illustrated in Fig. 20(c). Compared with the above three one-dimensional examples, though the accuracy of the proposed method is somewhat reduced, its potential in dealing with high-dimensional problems has also been observed.

6. Concluding remarks

In this paper, a novel approach for hybrid uncertainty propagation is proposed by integrating B-spline chaos with augmented change of probability measure (aCOM). Specifically, the considered issue of hybrid uncertainty propagation is compatible for both small and large epistemic uncertainties that characterize the uncertainty in the PDF of input random variables. To ensure the trade-off between efficacy and accuracy, the computation of B-spline chaos is conducted by partition of assigned-probability space throughout a GF-discrepancy minimization strategy. Main concluding remarks include:

(1) The versatility and flexibility of the proposed method is first illustrated by four benchmark problems. The accuracy and efficiency is further demonstrated by four numerical examples, taking analytical expressions or MCS results as reference solutions. The results indicate that the proposed method performs well for both linear and nonlinear models.

(2) The computational cost of the proposed method is dependent on the degree of epistemic uncertainty. Specifically, if the support of the original PDF fully covers the one of the updated PDF, no additional model evaluations are required. While if there is no overlap between the two PDFs, no improvement in efficiency can be achieved by the proposed method. This is referred to as a *no free lunch* situation.

(3) All the examined instances demonstrate that uncertainty in the input distribution may result in substantial uncertainty in the output distribution, in terms of shape and/or magnitude.

While most engineering practices are involved with high-dimensional random variables, the current method that deals with one-dimensional cases can be further improved at least by (1) adopting dimension reduction techniques, such as active subspace methods (adopted in this work), principal component analysis, sensitivity analysis, etc.; (2) developing multivariate B-spline chaos; (3) decoupling the original model into sub-models, e.g., high-dimensional model representation.

CRediT authorship contribution statement

Zhiqiang Wan: Writing – review & editing, Writing – original draft, Visualization, Validation, Methodology, Funding acquisition, Formal analysis, Conceptualization. **Weifeng Tao:** Writing – review & editing, Funding acquisition, Conceptualization. **Xiuli Wang:** Writing – review & editing, Investigation, Conceptualization. **Yuan Gao:** Validation, Software, Investigation.

Declaration of competing interest

The authors declare that they have no known competing financial interests or personal relationships that could have appeared to influence the work reported in this paper.

Data availability

Data will be made available on request.

Acknowledgments

The financial supports from the National Natural Science Foundation of China (NSFC Grant No. 52208206), the Natural Science Foundation of Shaanxi Province, China (Grant No. 2022JQ-513), and the Fundamental Research Funds for the Central Universities, China (Grant Nos. G2022KY05103, G2021KY05103) are highly appreciated.

Appendix A. The GF-discrepancy minimization strategy for point selection

The GF-discrepancy minimization strategy mainly includes three steps [19]:

Step A.1. Generate an initial point set. The initial point set can be obtained from the Sobol' sequence as suggested in [19] or via other methods. Let the Sobol' sequence be $S = \{u_q\}_{q=1}^N$ where $u_q \in [0, 1]$, then the initial point set of Θ denoted as $\mathcal{M}^{\text{ini}} = \{\theta_q^{\text{ini}}\}_{q=1}^N$ can be calculated by

$$\theta_q^{\text{ini}} = P_\Theta^{-1}(u_q),\ q = 1, \dots, N. \tag{A.1}$$

Step A.2. Rearrange each point from $\mathcal{M}^{\text{ini}} = \{\theta_q^{\text{ini}}\}_{q=1}^N$ by using the empirical CDF:

$$\theta_q^{\text{re}} = P_\Theta^{-1}\left(\sum_{k=1}^{N} \frac{1}{N} \cdot I\left(\theta_k^{\text{ini}} < \theta_q^{\text{ini}}\right) + \frac{1}{2} \cdot \frac{1}{N}\right),\ q = 1, \dots, N, \tag{A.2}$$

where $I(A) = 1$ if A holds true, otherwise $I(A) = 0$.

Step A.3. Rearrange each point from $\mathcal{M}^{\text{re}} = \{\theta_q^{\text{re}}\}_{q=1}^N$ by using the assigned probabilities:

$$\theta_q = P_\Theta^{-1}\left(\sum_{k=1}^{N} P_q \cdot I\left(\theta_k^{\text{re}} < \theta_q^{\text{re}}\right) + \frac{1}{2} \cdot P_q\right),\ q = 1, \dots, N, \tag{A.3}$$

where the assigned probability P_q is based on the definition in Eq. (8).

Strictly speaking, the above **Step A.3** should be performed multiple times (updating the assigned probabilities each time) to minimize the GF-discrepancy, but in general, relatively satisfactory results can be obtained after conducting **Step A.3** only once. The final optimal point set is $\mathcal{M} = \{\theta_q\}_{q=1}^N$. As for dependent random variables, the GF-discrepancy minimization-based point selection can be found in [43].

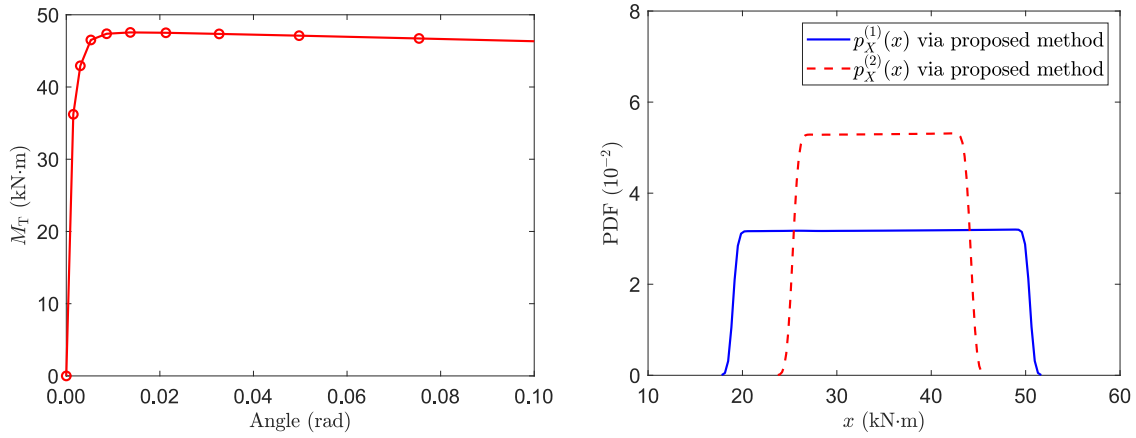

(a) A typical torque-angle curve via displacement method (b) PDFs of the torsion capacity

Fig. 19. Uncertainty quantification of a wind turbine tower model of two dry-joined circular ring segments (Example 3).

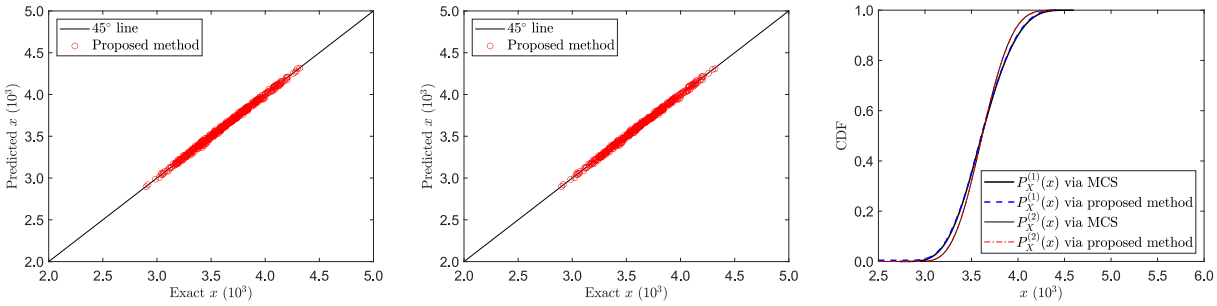

(a) Cross-validation (Problem 1) (b) Cross-validation (Problem 2) (c) CDFs of X

Fig. 20. Hybrid uncertainty propagation of the Golinski's speed reducer (Example 4).

Appendix B. Proof on the augmented change of probability measure

The proof that $\{\theta_q^{(2)}\}_{q=1}^{N+N_{\text{aug}}} \sim p_\Theta^{(2)}(\theta)$ via aCOM is given based on the composition method for generation of random variables [44]. Define $p_\Theta^{(1)}(\theta)$ and $p_\Theta^{(2)}(\theta)$ be expressed as mixture distributions, i.e.,

$$p_\Theta^{(1)}(\theta) = \pi_a^{(1)} \cdot p_{\Theta,a}^{(1)}(\theta) + \pi_b^{(1)} \cdot p_{\Theta,b}^{(1)}(\theta),\ \theta \in \Omega, \tag{B.1a}$$

$$p_\Theta^{(2)}(\theta) = \pi_a^{(2)} \cdot p_{\Theta,a}^{(2)}(\theta) + \pi_b^{(2)} \cdot p_{\Theta,b}^{(2)}(\theta),\ \theta \in \Omega, \tag{B.1b}$$

where

$$p_{\Theta,a}^{(1)}(\theta) = \frac{1}{\pi_a^{(1)}} \cdot p_\Theta^{(1)}(\theta),\ \theta \in \Omega_{\text{aug}}, \tag{B.2a}$$

$$p_{\Theta,b}^{(1)}(\theta) = \frac{1}{\pi_b^{(1)}} \cdot p_\Theta^{(1)}(\theta),\ \theta \in \Omega\backslash\Omega_{\text{aug}}, \tag{B.2b}$$

$$p_{\Theta,a}^{(2)}(\theta) = \frac{1}{\pi_a^{(2)}} \cdot p_\Theta^{(2)}(\theta),\ \theta \in \Omega_{\text{aug}}, \tag{B.2c}$$

$$p_{\Theta,b}^{(2)}(\theta) = \frac{1}{\pi_b^{(2)}} \cdot p_\Theta^{(2)}(\theta),\ \theta \in \Omega\backslash\Omega_{\text{aug}}, \tag{B.2d}$$

where $\pi_a^{(1)} = \int_{\Omega_{\text{aug}}} p_\Theta^{(1)}\mathrm{d}\theta$, $\pi_b^{(1)} = \int_{\Omega\backslash\Omega_{\text{aug}}} p_\Theta^{(1)}\mathrm{d}\theta$, $\pi_a^{(2)} = \int_{\Omega_{\text{aug}}} p_\Theta^{(2)}\mathrm{d}\theta$, and $\pi_b^{(2)} = \int_{\Omega\backslash\Omega_{\text{aug}}} p_\Theta^{(2)}\mathrm{d}\theta$.

Meanwhile, the augmenting PDF in Eq. (18) can be rewritten by

$$p_{\Theta,a}^{(2)}(\theta) = \frac{\pi_a^{(1)}}{\pi_a^{(2)}} \cdot p_{\Theta,a}^{(1)}(\theta) + \frac{\pi_a^{(2)} - \pi_a^{(1)}}{\pi_a^{(2)}} p_\Theta^{(\text{aug})}(\theta). \tag{B.3}$$

From Eq. (B.1a), a number of N_a samples from $\{\theta_q^{(1)}\}_{q=1}^{N}$ located in Ω_{aug} follow $p_{\Theta,a}^{(1)}(\theta)$. Since additional samples $\{\theta_q^{(2)}\}_{q=1}^{N_{\text{aug}}}$ are drawn from $p_\Theta^{(\text{aug})}(\theta)$, according to Eq. (B.3), there are $N_a + N_{\text{aug}}$ samples follow $p_{\Theta,a}^{(2)}(\theta)$. Note that from $\{\theta_q^{(1)}\}_{q=1}^{N}$ there are $N_b = N - N_a$ samples still remained in $\Omega\backslash\Omega_{\text{aug}}$, waiting to be equipped with new assigned probabilities, namely, N_b samples from $\{\theta_q^{(1)}\}_{q=1}^{N}$ will follow $p_{\Theta,b}^{(2)}(\theta)$ via aCOM. Due to the fact that $\Omega = \Omega_{\text{aug}} \cup \Omega\backslash\Omega_{\text{aug}}$ and from Eq. (B.1b), it is now clear that the new representative point set $\{\theta_q^{(2)}\}_{q=1}^{N+N_{\text{aug}}}$ on the definition of Eq. (19) via aCOM follow the distribution $p_\Theta^{(2)}(\theta)$. □

Appendix C. Active subspace method for dimension reduction

Consider Eq. (1) with $\boldsymbol{\Theta} \in \mathbb{R}^s$ where $s \geq 2$. Then, the uncentered covariance $\mathbf{C}$ can be computed by

$$\mathbf{C} = \int_{\Omega_{\boldsymbol{\Theta}}} \left(\nabla_{\theta} g\right) \left(\nabla_{\theta} g\right)^{\top} p_{\boldsymbol{\Theta}}(\boldsymbol{\theta}) \mathrm{d}\boldsymbol{\theta} \in \mathbb{R}^{s \times s}, \tag{C.1}$$

where $p_{\boldsymbol{\Theta}}(\boldsymbol{\theta})$ is the joint PDF of $\boldsymbol{\Theta}$, and $\nabla_{\theta} g = \left[\frac{\partial g}{\partial \theta_1}, \cdots, \frac{\partial g}{\partial \theta_s}\right]^{\top} \in \mathbb{R}^s$ is the gradient of g. Further, the eigenvalue decomposition of $\mathbf{C}$ gives that

$$\mathbf{C} = \mathbf{W} \boldsymbol{\Lambda} \mathbf{W}^{\top}, \tag{C.2}$$

in which $\mathbf{W} \in \mathbb{R}^{s \times s}$ and $\boldsymbol{\Lambda} \in \mathbb{R}^{s \times s}$ are eigenvector matrix and eigenvalue matrix with diagonal eigenvalues $\{\lambda_1, \ldots, \lambda_s\}$ satisfying that $\lambda_1 \geq \lambda_2 \geq \cdots \geq \lambda_s \geq 0$, respectively.

If $|\lambda_1 - \lambda_2|$ is far greater than the absolute difference between any other two adjoint eigenvalues, i.e., $|\lambda_1 - \lambda_2| \gg |\lambda_j - \lambda_{j+1}|$ for $j \in \{2, \ldots, s\}$ (consider $\lambda_{s+1} = 0$), one can find a one-dimensional active subspace defined by [27]

$$\hat{\theta} = \hat{\mathbf{W}}^{\top} \boldsymbol{\theta} \in \mathbb{R}^1, \tag{C.3}$$

where $\hat{\mathbf{W}}$ is the first column of $\mathbf{W}$. Let the approximation of $g(\boldsymbol{\theta})$ by $\tilde{g}(\hat{\theta})$. It has been proved that [27]

$$\mathbb{E}\left[\left(g(\boldsymbol{\theta}) - \tilde{g}(\hat{\theta})\right)^2\right] \leq \mathcal{L} \sum_{i=2}^{s} \lambda_s, \tag{C.4}$$

where $\mathcal{L}$ is the Lipschitz constant. In this work, we take advantage of the ASM to deal with high-dimensional cases. Moreover, the gradient-free algorithm [45,46] is adopted to calculate the uncentered matrix $\mathbf{C}$.

References

[1] Ang AHS, Tang W. Probability concepts in engineering: Emphasis on applications to civil and environmental engineering. Hoboken: John Wiley & Sons; 2007.

[2] Der Kiureghian A, Ditlevsen O. Aleatory or epistemic? Does it matter? Struct Saf 2009;31:105–12. http://dx.doi.org/10.1016/j.strusafe.2008.06.020.

[3] Ghanem R, Higdon D, Owhadi H, editors. Handbook of uncertainty quantification. Handbook of uncertainty quantification. Switzerland: Springer International Publishing; 2017, http://dx.doi.org/10.1007/978-3-319-12385-1.

[4] Chen JB, Wan ZQ. A compatible probabilistic framework for quantification of simultaneous aleatory and epistemic uncertainty of basic parameters of structures by synthesizing the change of measure and change of random variables. Struct Saf 2019;78:76–87. http://dx.doi.org/10.1016/j.strusafe.2019.01.001.

[5] Moore RE, Kearfott RB, Cloud MJ. Introduction to interval analysis. Philadelphia: Society for Industrial and Applied Mathematics; 2009, http://dx.doi.org/10.1016/0016-0032(67)90590-x.

[6] Valdebenito MA, Yuan X, Faes MG. Augmented first-order reliability method for estimating fuzzy failure probabilities. Struct Saf 2023;105:102380. http://dx.doi.org/10.1016/j.strusafe.2023.102380.

[7] Jerez DJ, Fragkoulis VC, Ni P, Mitseas IP, Valdebenito MA, Faes MG, Beer M. Operator norm-based determination of failure probability of nonlinear oscillators with fractional derivative elements subject to imprecise stationary Gaussian loads. Mech Syst Signal Process 2024;208:111043. http://dx.doi.org/10.1016/j.ymssp.2023.111043.

[8] Beer M, Ferson S, Kreinovich V. Imprecise probabilities in engineering analyses. Mech Syst Signal Process 2013;37:4–29. http://dx.doi.org/10.1016/j.ymssp.2013.01.024.

[9] Graf W, Götz M, Kaliske M. Analysis of dynamical processes under consideration of polymorphic uncertainty. Struct Saf 2015;52:194–201. http://dx.doi.org/10.1016/j.strusafe.2014.09.003.

[10] Faber MH. On the treatment of uncertainties and probabilities in engineering decision analysis. J Offshore Mech Arct Eng 2005;127:243–8. http://dx.doi.org/10.1115/1.1951776.

[11] Schöbi R, Sudret B. Uncertainty propagation of p-boxes using sparse polynomial chaos expansions. J Comput Phys 2017;339:307–27. http://dx.doi.org/10.1016/j.jcp.2017.03.021.

[12] Zhang JX, Shields MD. Efficient Monte Carlo resampling for probability measure changes from Bayesian updating. Probab Eng Mech 2019;55:54–66. http://dx.doi.org/10.1016/j.probengmech.2018.10.002.

[13] Wan ZQ, Hong X, Tao WF. Improvements to the probability density evolution method integrated with the change of probability measure on quantifying hybrid uncertainties. Struct Saf 2023;103:102342. http://dx.doi.org/10.1016/j.strusafe.2023.102342.

[14] Faes MG, Daub M, Marelli S, Patelli E, Beer M. Engineering analysis with probability boxes: A review on computational methods. Struct Saf 2021;93:102092. http://dx.doi.org/10.1016/j.strusafe.2021.102092.

[15] Eckert C, Beer M, Spanos PD. A polynomial chaos method for arbitrary random inputs using B-splines. Probab Eng Mech 2020;60:103051. http://dx.doi.org/10.1016/j.probengmech.2020.103051.

[16] Rahman S. A spline chaos expansion. SIAM/ASA J Uncertain Quantif 2020;8(1):27–57. http://dx.doi.org/10.1137/19M1239702.

[17] Wan XL, Karniadakis GE. An adaptive multi-element generalized polynomial chaos method for stochastic differential equations. J Comput Phys 2005;209:617–42. http://dx.doi.org/10.1016/j.jcp.2005.03.023.

[18] Nguyen VP, Anitescu C, Bordas SP, Rabczuk T. Isogeometric analysis: An overview and computer implementation aspects. Math Comput Simulation 2015;117:89–116. http://dx.doi.org/10.1016/j.matcom.2015.05.008.

[19] Chen JB, Yang JY, Li J. A GF-discrepancy for point selection in stochastic seismic response analysis of structures with uncertain parameters. Struct Saf 2016;59:20–31. http://dx.doi.org/10.1016/j.strusafe.2015.11.001.

[20] Chen JB, Ghanem R, Li J. Partition of the probability-assigned space in probability density evolution analysis of nonlinear stochastic structures. Probab Eng Mech 2009;24:27–42. http://dx.doi.org/10.1016/j.probengmech.2007.12.017.

[21] Chen JB, Chan JP. Error estimate of point selection in uncertainty quantification of nonlinear structures involving multiple nonuniformly distributed parameters. Internat J Numer Methods Engrg 2019;118:536–60. http://dx.doi.org/10.1002/nme.6025.

[22] Li J, Wang D. Comparison of PDEM and MCS: Accuracy and efficiency. Probab Eng Mech 2023;71:103382. http://dx.doi.org/10.1016/j.probengmech.2022.103382.

[23] Grigoriu M. Stochastic calculus: Applications in science and engineering. New York: Springer Science+Business Media; 2002.

[24] Fan WL, Ang AHS, Li ZL. Reliability assessment of deteriorating structures using Bayesian updated probability density evolution method (PDEM). Struct Saf 2017;65:60–73. http://dx.doi.org/10.1016/j.strusafe.2016.12.004.

[25] Wan ZQ, Chen JB, Li J, Ang AHS. An efficient new PDEM-COM based approach for time-variant reliability assessment of structures with monotonically deteriorating materials. Struct Saf 2020;82:101878. http://dx.doi.org/10.1016/j.strusafe.2019.101878.

[26] Rashki M, Faes MGR. No-free-lunch theorems for reliability analysis. ASCE-ASME J Risk Uncertain Eng Syst A 2023;9(3):04023019. http://dx.doi.org/10.1061/ajrua6.rueng-1015.

[27] Constantine PG, Dow E, Wang QQ. Active subspace methods in theory and practice: Applications to kriging surfaces. SIAM J Sci Comput 2014;36(4):A1500–24. http://dx.doi.org/10.1137/130916138.

[28] Marrel A, Iooss B, Laurent B, Roustant O. Calculations of sobol indices for the Gaussian process metamodel. Reliab Eng Syst Saf 2009;94:742–51. http://dx.doi.org/10.1016/j.ress.2008.07.008.

[29] Schueremans L, Van Gemert D. Benefit of splines and neural networks in simulation based structural reliability analysis. Struct Saf 2005;27:246–61. http://dx.doi.org/10.1016/j.strusafe.2004.11.001.

[30] Jiang ZM, Li J. High dimensional structural reliability with dimension reduction. Struct Saf 2017;69:35–46. http://dx.doi.org/10.1016/j.strusafe.2017.07.007.

[31] Rehme MF, Franzelin F, Pflüger D. B-splines on sparse grids for surrogates in uncertainty quantification. Reliab Eng Syst Saf 2021;209:107430. http://dx.doi.org/10.1016/j.ress.2021.107430.

[32] Rahman S, Jahanbin R. A spline dimensional decomposition for uncertainty quantification in high dimensions. SIAM-ASA J Uncertain Quantif 2022;10(1):404–38. http://dx.doi.org/10.1137/20M1364175.

[33] Soize C, Ghanem R. Probabilistic-learning-based stochastic surrogate model from small incomplete datasets for nonlinear dynamical systems. Comput Methods Appl Mech Engrg 2024;418:116498. http://dx.doi.org/10.1016/j.cma.2023.116498.

[34] Tao WF, Li J. An ensemble evolution numerical method for solving generalized density evolution equation. Probab Eng Mech 2017;48:1–11. http://dx.doi.org/10.1016/j.probengmech.2017.03.001.

[35] Wang D, Sun WL, Li J. An RKPM-based formulation of the generalized probability density evolution equation for stochastic dynamic systems. Probab Eng Mech 2021;66:103152. http://dx.doi.org/10.1016/j.probengmech.2021.103152.

[36] Lyu MZ, Feng DC, Chen JB, Li J. A decoupled approach for determination of the joint probability density function of a high-dimensional nonlinear stochastic dynamical system via the probability density evolution method. Comput Methods Appl Mech Engrg 2024;418:116443. http://dx.doi.org/10.1016/j.cma.2023.116443.

[37] Li J, Chen JB. Stochastic dynamics of structures. Singapore: John Wiley & Sons; 2009, http://dx.doi.org/10.1002/9780470824269.

[38] Jiang ZM, Li J. Analytical solutions of the generalized probability density evolution equation of three classes stochastic systems. Chin J Theor Appl Mech 2016;48(2):413–21. http://dx.doi.org/10.6052/0459-1879-15-221.

[39] Song JW, Wei PF, Valdebenito MA, Faes M, Beer M. Data-driven and active learning of variance-based sensitivity indices with Bayesian probabilistic integration. Mech Syst Signal Process 2022;163:108106. http://dx.doi.org/10.1016/j.ymssp.2021.108106.

[40] Wan ZQ. Global sensitivity evolution equation of the Fréchet-derivative-based global sensitivity analysis. Struct Saf 2024;106:102413. http://dx.doi.org/10.1016/j.strusafe.2023.102413.

[41] Loh L, Garg A. Torsionstragverhalten von betonhohlquerschnitten in geschlossenen und klaffenden segmentfugen – teil 3: Verifikation des berechnungsmodells. Beton- Stahlbetonbau 2023;118:417–26. http://dx.doi.org/10.1002/best.202300003.

[42] Jiang X, Hu XZ, Liu G, Liang X, Wang RL. A generalized active subspace for dimension reduction in mixed aleatory-epistemic uncertainty quantification. Comput Methods Appl Mech Engrg 2020;370:113240. http://dx.doi.org/10.1016/j.cma.2020.113240.

[43] Yang JY, Tao JJ, Sudret B, Chen JB. Generalized F-discrepancy-based point selection strategy for dependent random variables in uncertainty quantification of nonlinear structures. Internat J Numer Methods Engrg 2020;121:1507–29. http://dx.doi.org/10.1002/nme.6277.

[44] Law AM. Simulation modeling and analysis. 5th ed.. New York: McGraw-Hill; 2015.

[45] Hokanson JM, Constantine PG. Data-driven polynomial ridge approximation using variable projection. SIAM J Sci Comput 2018;40(3):A1566–89. http://dx.doi.org/10.1137/17M1117690.

[46] Wan ZQ, Chen JB, Tao WF, Wei PF, Beer M, Jiang ZM. A feature mapping strategy of metamodelling for nonlinear stochastic dynamical systems with low to high-dimensional input uncertainties. Mech Syst Signal Process 2023;184:109656. http://dx.doi.org/10.1016/j.ymssp.2022.109656.